DESIGNING A MACROSCOPIC SINGLET-TRIPLET QUBIT IN A LINEAR ARRAY OF QUANTUM DOTS EMBEDDED IN NANOWIRES

By
Nick Rogers
January 2016

A Thesis
submitted to the School of Graduate Studies and Research
in partial fulfillment of the requirements
for the degree of
Master of Science in Physics[1]

[1]The M.Sc. Program is a joint program with Carleton University, administered by the Ottawa-Carleton Institute of Physics

Abstract

In this thesis I present a theory of a macroscopic singlet-triplet qubit in quantum dots embedded in nanowires, each containing 4 electrons and together simulating an artficial Haldane gap material. A Haldane gap material exhibits a 4-fold degenerate ground state separated by an energy gap from excitations. The ground state is equivalent to a degenerate spin-singlet and -triplet state. The 4 degenerate states exhibit the characteristics of spins-1/2 localized on either end of the chain. These states may be used as a coded qubit for quantum information processing.

Using the effective mass approximation, I calculate single-particle energy levels of one and two quantum dots in a quantum wire. Using these energy levels I compute the Coulomb matrix elements of the interacting Hamiltonian. Using configuration interaction I demonstrate that the ground state of a quantum dot with 4 electrons is a spin-1 state. I then show that the two dot system behaves approximately like two spin-1 objects interacting via an antiferromagnetic Heisenberg Hamiltonian. While the Heisenberg model is approximate, the two dots have a spin-0 ground-state, indicating antiferromagnetic coupling. I then present a simpler spin model to illustrate the physical parameters which control this interaction. Finally, I present a brief solution to the Heisenberg Hamiltonian for finite spin-chains, and show how one can manipulate the singlet-triplet combined ground state of the spin-chain via localized magnetic field, realizing a singlet-triplet qubit in a macroscopic semiconductor device.

Acknowledgements

I would first and foremost like the thank my thesis advisor, Dr. Pawel Hawrylak—without whom none of this would have been possible—for the majority of the motivation and background of everything I have done, for regular lengthy discussions of procedure and results, as well as for giving me an intuition for some concepts I never could have imagined having.

I would also like to thank my co-supervisor Dr. Thomas Brabec for making the whole thing possible, for which I am extraordinarily grateful.

Further, I would like to thank Dr. Marek Korkusinski for very patiently explaining concepts in about the easiest-to-understand manner one could hope for, as well as Isil Ozfidan for excellent advice and particularly for reminding me not to overcomplicate things. Finally, I would like to thank the rest of our group, past and present—Milos Vladisavljevic and Julien Thibert-Leduc—as well as our numerous visiting students and professors over the last two years for insightful discussions and coffee.

I would like to thank my family and friends for regularly asking me what my thesis is about. In attempting to explain my work to anyone and everyone I have been able to solidify my own understanding; my explanation gets better every time and this sort of exercise is invaluable. I would also like to thank Nate for lending me his GameCube controllers indefinitely.

I dedicate this work to whomever finds it useful.

Notes

It is cumbersome to put multiple indices on a variable as subscripts, so occasionally I will use superscripts. In particular, in my discussion of spins on a lattice site i, I will put the Cartesian spin component in a superscript, *e.g.* S_i^z. Elsewhere, where only the Cartesian component is needed, I will refer to S_{tot}^z, S^z, or perhaps S_z. Any ambiguity should be self-clarifying.

Contents

Chapter 1

Introduction

The spin-chain Heisenberg Hamiltonian describes a 1D lattice of interacting spins. The interaction of the spins is characterized by a strength J, which is the only parameter in the model. When J is positive, this interaction is *antiferromagnetic*, tending to anti-align neighboring spins (while for a negative J it is ferromagnetic). Interest in antiferromagnetic integer-spin chains came about in 1983 when F.D.M. Haldane, based on field-theoretical reasoning, postulated that the ground-state is separated from excitation by an energy gap[1]. Before being proven theoretically by Affleck et al. in 1988[2], this postulate was strongly supported throughout the 1980's by finite-chain calculations[3] and experiments on, for example, $CsNiCl_3$[4].

The field remains active and promising to this day; mainly in the context of semiconductor nanostructures intended to mimic the lattice-bound spin-1 particles by taking advantage of the electronic or excitonic correlations in quantum dots. For example, a recent paper proposes loading gated lateral quantum dot molecules with controlled electron numbers in such a way that the molecule will have a collective spin-1 ground state and interact weakly with neighboring molecules antiferromagnetically[5]. Such gated quantum dots, however, are very weakly bound, leading to Haldane gaps of $E_g/k_B \lesssim 50$ mK[5].

In this thesis I propose to realize a Haldane gap material in a linear array of quantum dots embedded in nanowires and loaded with 4 electrons each. There are many reasons to favour such a design; not the least of which being a potentially large

Haldane gap.

1.1 The Spin-1 Heisenberg Hamiltonian and the Haldane Gap

The (antiferromagnetic) Heisenberg Hamiltonian for N spins is

$$H_{Heis} = J \sum_{i=1}^{N-1} \boldsymbol{S}_i \cdot \boldsymbol{S}_{i+1}, \tag{1.1}$$

where $J > 0$ is the spin-spin interaction and S_i is the spin S on site i.

As each site has $(2S+1)$ states $|S_i^z\rangle$, the basis is of size $(2S+1)^N$, where S is the spin of each site. This quickly becomes very large. The configurations are of course all degenerate in the absence of J.

This Hamiltonian has unique properties when the spins are integer-valued and in particular when $S = 1$. In finite chains, the ground state will have total spin 0 or 1 for even or odd chains, respectively (as might seem obvious given the tendency of adjacent pairs to antialign), and as the chain becomes longer, these four levels ($S = 0$ singlet and $S = 1$ triplet) become closer and closer in energy, becoming degenerate in an infinite chain. Moreover, these four states become separated from the next excitation, an $S = 2$ quintuplet, by a sizeable energy gap that also persists in an infinite chain (achieving a value of $\sim 0.41J$[6]). This energy gap is known as the *Haldane gap*, and it and the ground state it isolates have been the subject of great interest since they were first discovered.

The degenerate singlet and three triplet states that form the ground state can be imagined as isolated (and noninteracting) quasiparticles of spin $S = 1/2$ located one at each edge of the chain[7]. Indeed, in finite-chain calculations one finds that $\langle S_i^z \rangle = 0.5$ on the first and N^{th} lattice sites. Importantly and somewhat to this point, the 4-fold degenerate ground state is a 1-to-1 representation of a *singlet-triplet qubit*[8][9]. Qubits are two-state quantum systems that serve as a basis for quantum computing manipulations. The conventional singlet-triplet qubit makes use of two of the four total S^2 eigenstates of two of spin-1/2 particles.

Much work has been done towards the creation and manipulation of these singlet-triplet qubits, where the $S_z = \pm 1$ triplet states $|T_\pm\rangle$ are split from the $S_z = 0$ singlet and triplet states $|S_0\rangle$ and $|T_0\rangle$ by application of a uniform magnetic field, and the $|S_0\rangle$ and $|T_0\rangle$ levels are mixed and manipulated by an anisotropy of the nuclear magnetic field. This could potentially be realized in a finite spin-chain as well.

Finally, the presence of the energy gap isolating these qubits from excitation makes the system relatively robust, provided that a physical system with a large effective J can be found or engineered. Early experiments on integer spin chains were performed on $CsNiCl_3$[4], but more recently there has been interest in designing these spin-chains using semiconductor nanostructures, so that one can tune the properties of the system in order to maximize J. This thesis explores one such nanostructure, but I will first introduce the concept of nanostructures—particularly quantum dots and quantum nanowires—in general.

1.2 Quantum Dots

Quantum dots are nanostructures that confine quasiparticles in all three spatial dimensions. Contrast this with *quantum wells* that are quasi-2D, confining in one spatial dimension—for example, a large graphene flake—and quasi-1D *quantum wires* confining in two spatial dimensions—for example, III-V nanowires. Quantum dots are often called *zero-dimensional* in keeping with the terminology, though this can be misleading as they retain some spatial characteristics. The terminology is meant to elucidate the notion that quasiparticles in a quantum dot are *confined* in all three dimensions spatially.

Some examples of quantum dots include colloidal quantum dots, which are nanoparticles of, *e.g.*, gold, perhaps hundreds of nanometers in diameter. As another example, a small amount of impurity material embedded in a host semiconductor, *e.g.*, InAs embedded in InP, can form a potential minimum, confining particles much like an atom confines electrons.

In a bulk semiconductor exhibiting no confinement the energy levels of quasiparticles are closely-spaced enough to be described by a continuous dispersion relation.

In quantum dots, however, energy levels are highly quantized. As a consequence, when multiple particles occupy a dot at once, Pauli exclusion becomes important and they begin to fill levels in analogy to Hund's rules in atoms; the energy levels can be thought of as forming *shells*, and they are filled lowest first, with single occupation within a shell preceding double occupation[10][11].

Much like how electrons and holes in bulk semiconductors are often well approximated about the band edge by a k^2 (free particle) dispersion relation with an effective mass m^*, quantum dots are often quite well approximated by potential minima to such a particle. In particular, lens-shaped self-assembled quantum dots (nucleated structures grown on top of a lattice-mismatched semiconductor) have spectra that fit extraordinarily well with a 2D quantum harmonic oscillator[12][13], capturing the level spacing, degeneracies, and effect of magnetic field; while nonparabolic, roughly-cylindrical quantum structures are quite well described by cylindrical potential wells[12].

Quantum dots are much more desirable than structures found in nature simply for the fact that their energetic properties can be tuned by controllable parameters. For example, the difference in bandgap between the two semiconductors controls the depth of the potential well. This can be tuned, for example, by increasing the arsenic content of an InAsP dot embedded in InP. Further, energy level spacing has an inverse dependence on dot size—*e.g.* a 1D square well has energy levels E_n proportional to $n^2\pi^2/L^2$, where L is its length—smaller dots have larger level spacing. By controlling the size of the dot and the bandgap difference, the separation between levels and interactions between particles on these levels can be engineered. Many growth techniques allow tuning of dot height and width to a great degree of precision[14].

1.2.1 Energetics of Quantum Dots

As the 2D harmonic oscillator is the archetypical model for a quantum dot in the effective mass approximation, I will refer to it here, however the discussion on the

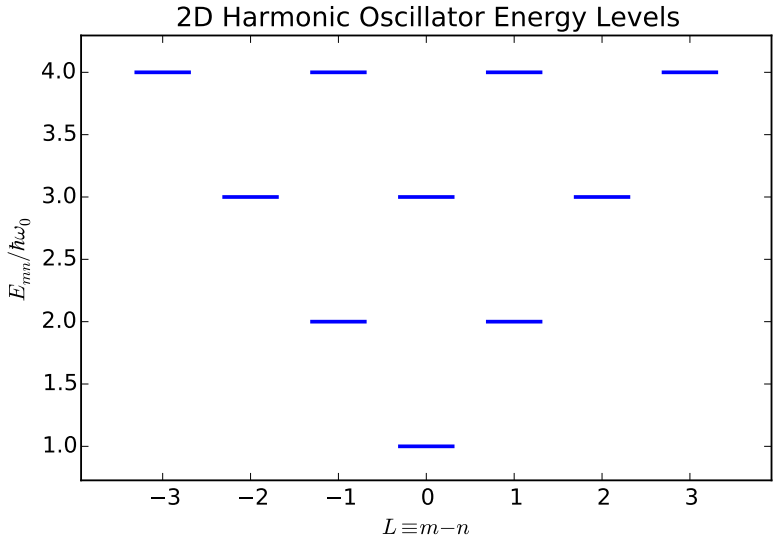

Figure 1.1: Ladder of the first few 2D Harmonic oscillator levels. In analogy with atoms, the lowest level is referred to as the s-shell, followed by the two-fold degenerate p-shell, the 3-fold degenerate d-shell, the 4-fold degenerate f-shell, etc; in general, the n-fold degenerate n^{th} shell. The quantum numbers are $\{n, m\} \in 0, 1, 2, \ldots$; increasing n (m) move up one unit of $\hbar\omega_0$ and to the left (right) one quantum of angular momentum.

whole will be analogous for any system with similar symmetry (in particular cylindrical potential wells, especially at lower energies, have a very similar spectrum). The 2D harmonic oscillator with characteristic frequency ω_0 is described by the Hamiltonian

$$H = \frac{\hbar^2 \hat{k}^2}{2m^*} + \frac{1}{2} m^* \omega_0^2 \hat{x}^2 + \frac{1}{2} m^* \omega_0^2 \hat{y}^2 \tag{1.2}$$

where m^* is the effective mass of the particle. This has the well-known energy levels

$$E = \hbar\omega_0 \left(n + \frac{1}{2} \right) + \hbar\omega_0 \left(m + \frac{1}{2} \right) \tag{1.3}$$

for x, y modes $n, m \in \{0, 1, 2, \ldots\}$. This is a pleasing solution in a few ways; the levels are evenly spaced, and form degenerate *shells*; with the n^{th} shell being n-fold degenerate. They are customarily enumerated in analogy with atomic shells (*spdf*...). The quantity $m - n$ turns out to represent in-plane orbital angular momentum[15].

When we begin to load these levels with few particles, they tend to prefer spin configurations governed by Hund's rules; that is, the energetically favourable total

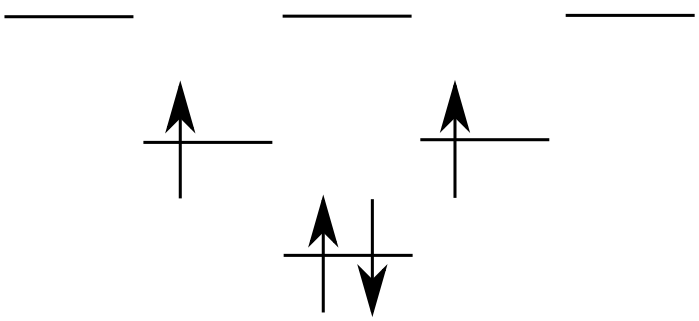

Figure 1.2: Schematic illustration of Hund's rules filling of harmonic oscillator levels for 4 electrons. The energetically favourable spin configuration is consistent with this picture of shell-filling.

spin is consistent with level filling by single occupation within a shell followed by double occupation within a shell, in turn followed by single-occupation in the next shell, and so on. We should then, after a brief glance at Figure 1.1, expect that two electrons on such a quantum dot will form a spin-singlet, the main configuration thereof fully occupying the s-shell, since the s-shell only has a single state. Due to the Coulomb exchange interaction between aligned spins the third and fourth electron will form a spin-triplet state. Indeed, this is precisely what happens, as I will show for the cylindrical potential well in Section 3.2.2. There is extensive literature on the subject as it pertains to the harmonic oscillator, *e.g.* ref. [16].

One can tune the spectrum of a quantum dot by introducing perturbing effects into the Hamiltonian. A drastic example is the introduction of a very strong magnetic field, which creates an anisotropy between the characteristic frequencies of the two harmonic modes. In this way, the spectrum can be split into *Landau levels*, which are essentially ladders of levels with increasing L; energy levels within a Landau level are separated by the smaller of the two characteristic frequencies $\hbar\omega$ and the bottom of the Landau levels themselves are separated by the (typically much) larger frequency larger $\hbar\Omega$. The multiparticle spectrum of such a system is much different, and leads to some rather interesting effects[15].

The harmonic oscillator is a very good model for lens-shaped self-assembled quantum dots (SAQD's), which have been studied in great detail both experimentally and theoretically[13][17]. In particular, the evolution of the dot emission as a function of

magnetic field corresponds incredibly well to the spectrum of a 2D harmonic oscillator potential[13]. It has also been shown experimentally that the energetics of these dots are highly sensitive to the number of electrons or *excitons* (bound electron-hole pairs) in the dot; an indication the "artificial atom" character of these systems[13].

1.2.2 Quantum Dot Molecules and Heterostructures

Keeping with the atom analogy, quantum dots can interact with one another to form *artificial molecules*[18][19], opening up the possibility for countless heterostructure architectures. Gated lateral quantum dot molecules (where the potential minima are tuned by a voltage, allowing precise control of electron occupation number) have been studied experimentally and theoretically in great detail; typically via a linear combination of harmonic orbitals (LCHO) method completely analogous to the LCAO of quantum chemistry[19][20].

Another heterostructure—the basis of this thesis—is the linear array of vertically-coupled quantum dots. Under certain conditions; namely, with each dot having 4 electrons (recall this tends to form a spin-1 ground state), and when the interdot interaction is weak compared to the on-site Coulomb exchange keeping each quantum dot in a spin-1 state, the low-energy spectrum of two such dots is well-approximated by the N=2 Heisenberg Hamiltonian (1.1) for spins-1[5][21].

While vertically-coupled quantum dots have been studied before, their in-plane character is often treated as a harmonic oscillator potential, since this is both easiest to work with and best understood[21][22]. In *nanowires*, the quantum dot is better modeled by cylindrical potentials. These systems have also been studied, but in quite a bit less detail[23].

1.2.3 Nanowire Quantum Dots

Nanowires are quasi-one-dimensional semiconductors; contrasted with quantum dots, nanowires exhibit a quasicontinuum of levels along one spatial dimension. They are grown predominantly using epitaxial methods that in some way control the area of growth; for example, catalyzed vapour-liquid-solid (VLS) epitaxy, where a catalyst

particle is placed on the wetting layer and growth occurs only directly below the catalyst. By changing the deposition vapour partway through the growth process, one can embed a quantum dot in the nanowire.

Through a combination of epitaxial methods (VLS and selective-area deposition) nanowires can be grown with very few stacking faults, and hence very pure emission from confined dot states can be observed[14]. The dot height can be tuned to atomic precision by changing deposition time, and the dot radius is determined by the size of the catalyst particle. By controlling both of these physical properties one can engineer the shell structure of the quantum dot.

Characterization of multiple nanowire quantum dots is scarce in the literature. The majority of the work has been limited to effective mass calculations. Ab initio calculations to account for strain have been performed, however the strain profile makes this a difficult calculation[24]. Full atomistic calculations have been performed on empty nanowires[25] and on single dots embedded in nanowires[26].

There is no reason that one cannot, in principle, grow such a nanowire with multiple embedded dots. Indeed, one might imagine that such a system would make an excellent candidate for a spin-chain. For one, the confining potential of these dots is on the order of 100 meV[14], which could potentially allow for a rather large Heisenberg J and hence a large Haldane gap. They exhibit cylindrical symmetry and can be constructed so that vertical levels do not play a role in the energetics of the system, somewhat mimicking the band structure of the harmonic ocillator potential which is known to have favourable spin-1 configurations.

1.3 Contents of This Thesis

As quantum dots embedded in nanowires seem to be a good candidate system for realizing a spin-1 chain, I will henceforth investigate their properties. The nanowire naturally provides an array-like structure for quantum dots, and the systems can be grown to extraordinary purity. In the following sections I will characterize such a quantum dot array under the effective mass approximation, to determine:

- Whether a single dot with 4 electrons has a spin-1 ground state;

- The spectrum of a two-dot system with 8 electrons, and whether it can be mapped onto the Heisenberg Hamiltonian;
- If the Heisenberg model is appropriate, what physical characteristics of the two-dot system determine its validity and the strength of interaction.

Following the characterization of the double-dot nanowire system I will look at spin-chains in general, first verifying previous finite-chain calculations, and then attempting to manipulate the ground states in order to realize a working singlet-triplet qubit. I will employ ideas that we have developed from understanding smaller systems (*e.g.* manipulating the singlet and triplet with an anisotropic magnetic field, which is routinely done with two spins but not immediately obviously applicable to a spin chain).

1.3.1 Statement of Originality

I present in this thesis many different theoretical models of particular quantum dot systems and spin chains. All of the calculations presented have been done by myself, and with the exception of the inclusion of standard numerical libraries and packages, all computation was done by myself.

Further, many parts of this thesis represent completely original work. Specifically, the following calculations have not been repeated or compared to any other results that may or may not exist in the literature:

- Single-particle levels in a 2-dot nanowire;
- 8-electron energy spectrum in a 2-dot nanowire;
- Determination of an effective Heisenberg Hamiltonian in a 2-dot nanowire;
- Dependence of Heisenberg model on dot parameters;
- Manipulation of spin-chains with localized magnetic fields.

The idea of implementing a spin-1 chain in semiconductors is not new, as it has been put forward in our group[5] though the proposal to implement such a chain specifically in nanowire quantum dots is unique.

Chapter 2

Single Particle Levels in Quantum Dots

There are number of approximations that can be used to determine the single-particle levels of a quantum dot system. The level of approximation directly corresponds to the level of detail about the system that is discarded. Of course, detailed atomistic calculations are rather intensive numerically, while effective mass systems often have analytic solutions. There is thus a tradeoff between accuracy and computational intensity. Nonetheless, the important characteristics of the geometry of many microstructural systems with sizes greater than several nanometers are well-approximated by an effective mass treatment. It is common to treat many systems (self-assembled quantum dots and gated quantum dots among others) as a 2D harmonic oscillator[10][12][19], perhaps with perturbations. This system has the advantage of a single-particle solution that has been known since the advent of quantum mechanics, and an analytical Coulomb matrix element[12][17]. Systems with hard cylindrical symmetry (well-modeled by a piecewise constant cylindrical potential, as opposed to soft cylindrical potentials, *i.e.* those well-modeled by the harmonic oscillator; such as lens-shaped systems) are better-approximated by finite or infinite cylindrical wells. The infinite cylinder is a slightly more complicated model than the harmonic oscillator, with no analytical solution for the Coulomb potential. Since all of the structures I am considering exhibit hard cylindrical geometry, I will focus on

cylindrical potential wells.

2.1 The Effective Mass Approximation and Rydberg Units

Through the rest of this thesis I will be focusing on results obtained from an effective mass treatment of quantum structures. This treatment approximates the dispersion relation of an electron in the material with a normal dispersion with an effective mass m^*; that is, the kinetic term in the Hamiltonian T is given by

$$\hat{T} = \frac{\hat{p}^2}{2m^*}, \tag{2.1}$$

where p is the usual momentum. In the systems I am considering, the quantum dot is formed in a material with a certain band gap embedded within another material with a larger one; for example, InAsP quantum dots in an InP nanowire[14].

Including a spatially-dependent potential $V(\mathbf{r})$ to model the quantum dot, the single-particle Hamiltonian will always be

$$\hat{H} = \frac{\hat{p}^2}{2m^*} + \hat{V}(\hat{\mathbf{r}}). \tag{2.2}$$

Further, I will here introduce the effective atomic (Rydberg) units.

The basic unit of length is the effective Bohr radius,

$$a_B = \frac{4\pi\epsilon\hbar^2}{m^* e^2} \approx \frac{m_0}{m^*}\frac{\epsilon}{\epsilon_0} \cdot 0.529 \text{ Å}, \tag{2.3}$$

where ϵ is the permittivity of the material, and m_0 is the reduced electron mass and 0.529 Å is the actual Bohr radius, and the basic unit of energy is the effective Rydberg,

$$\text{Ry} = \frac{\hbar^2}{2m^* a_B^2} \approx \frac{m^*}{m_0}\left(\frac{\epsilon_0}{\epsilon}\right)^2 \cdot 13.6 \text{ eV}, \tag{2.4}$$

where 13.6 eV is the binding energy of the ground state of Hydrogen.

Making the variable substitution

$$\tilde{\mathbf{r}} = \frac{\mathbf{r}}{a_B} \tag{2.5}$$

$$\frac{\partial^2}{\partial \tilde{r}_i^2} = a_B^2 \frac{\partial^2}{\partial r^2} \tag{2.6}$$

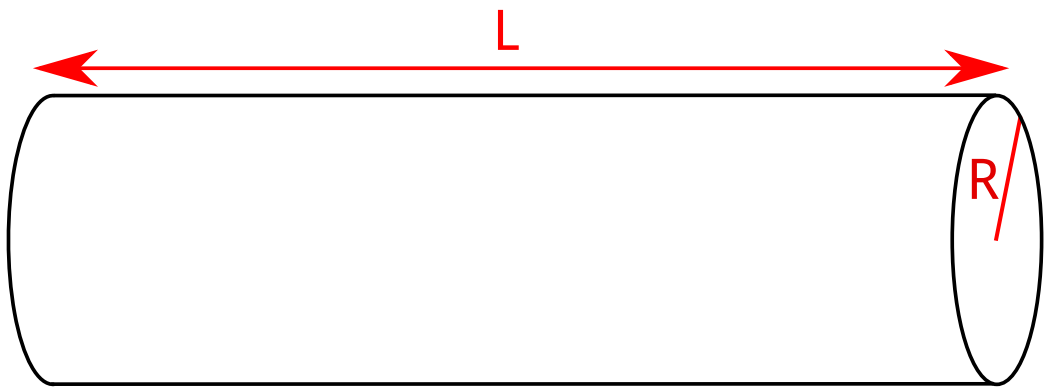

Figure 2.1: Illustration of a quantum wire.

and dividing the Hamiltonian (and of course the right-hand side of the Schrödinger equation) by the Rydberg, I am left with

$$\hat{H} = -\hat{\tilde{\nabla}}^2 + \hat{V}(\hat{\tilde{\mathbf{r}}}), \tag{2.7}$$

where everything with a tilde and the Hamiltonian itself are now dimensionless.

For a typical semiconductor, with $m^*/m_0 = 0.054$ and $\epsilon/\epsilon_0 = 12.4$, these quantities are $a_B = 12.15$ nm and Ry $= 4.776$ meV.

2.2 The Infinite Cylindrical Well: Quantum Disks and Quantum Nanowires

I start with the case of the infinite cylindrical well. This is a first approximation for an isolated cylindrically-symmetric material; it is appropriate for modeling disk-shaped quantum dots and nanowires. The solution of this problem will be used as a basis for further calculations.

The Hamiltonian in the position basis, in cylindrical coordinates (ρ, ϕ, z) is

$$H = -\nabla^2 + V_\rho(\rho) + V_z(z), \tag{2.8}$$

where

$$V_\rho(\rho) = \begin{cases} 0, & 0 \le \rho \le R; \\ \infty, & \text{otherwise}, \end{cases} \tag{2.9}$$

and

$$V_z(z) = \begin{cases} 0, & 0 \leq z \leq L; \\ \infty, & \text{otherwise.} \end{cases} \tag{2.10}$$

In cylindrical coordinates, the Laplacian operator is

$$\nabla^2 = \frac{1}{\rho}\frac{\partial}{\partial\rho}\left(\rho\frac{\partial}{\partial\rho}\right) + \frac{1}{\rho^2}\frac{\partial^2}{\partial\phi^2} + \frac{\partial^2}{\partial z^2}, \tag{2.11}$$

leaving me with the separable Hamiltonian

$$H = \left[-\frac{1}{\rho}\frac{\partial}{\partial\rho}\left(\rho\frac{\partial}{\partial\rho}\right) - \frac{1}{\rho^2}\frac{\partial^2}{\partial\phi^2} + V_\rho(\rho)\right] + \left[-\frac{\partial^2}{\partial z^2} + V_z(z)\right]. \tag{2.12}$$

Applying the Schrödinger equation

$$H\psi(\mathbf{r}) = E\psi(\mathbf{r}) \tag{2.13}$$

and limiting my solution space to the region where $V = 0$, after separating I have

$$E_r\psi_r = -\frac{1}{\rho}\frac{\partial}{\partial\rho}\left(\rho\frac{\partial}{\partial\rho}\right)\psi_r - \frac{1}{\rho^2}\frac{\partial^2}{\partial\phi^2}\psi_r \tag{2.14a}$$

$$E_z\psi_z = -\frac{d^2\psi_z}{dz^2} \tag{2.14b}$$

Because of my choice of boundary condition ($0 \leq z \leq L$), the latter (axial) part gives me sine functions only;

$$\psi_z = \sqrt{\frac{2}{L}}\sin\left(\frac{\ell\pi z}{L}\right); \quad \ell \in \{1, 2, 3, \ldots\}, \tag{2.15}$$

with energies

$$E_z = \frac{\ell^2\pi^2}{L^2}. \tag{2.16}$$

The former (radial) part is further separable; I first multiply by ρ^2 and move everything to one side, leaving

$$\left(\rho^2\frac{\partial^2\psi_r}{\partial\rho^2} + \rho\frac{\partial\psi_r}{\partial\rho} + \rho^2E_r\psi_r\right) + \frac{\partial^2\psi_r}{\partial\phi^2} = 0, \tag{2.17}$$

at which point I can separate by introducing the quantum number m;

$$\rho^2\frac{d^2\psi_\rho}{d\rho^2} + \rho\frac{d\psi_\rho}{d\rho} + \rho^2E_r\psi_\rho = m^2\psi_\rho \tag{2.18a}$$

$$\frac{d^2\psi_\phi}{d\psi_\phi^2} = -m^2\psi_\phi \tag{2.18b}$$

The latter is trivial and gives me complex exponentials;

$$\psi_\phi = \frac{1}{\sqrt{2\pi}} e^{im\phi}; \quad m \in \{0, \pm 1, \pm 2, \dots\} \tag{2.19}$$

which represent the in-plane orbital angular momentum of the wavefunction.

For the former, if I let $k = \sqrt{E_r}$, I can write

$$k^2\rho^2 \frac{d^2\psi_\rho}{d(k\rho)^2} + k\rho \frac{d\psi_\rho}{d(k\rho)} + (k^2\rho^2 - m^2)\psi_\rho = 0, \tag{2.20}$$

recovering the Bessel equation in $k\rho$. The general solution is

$$\psi_\rho = AJ_m(k\rho) + BY_m(k\rho); \tag{2.21}$$

that is, Bessel functions of the first and second kind, respectively. My boundary conditions (namely, the wavefunction must not diverge anywhere) specify that B must vanish as all $Y_m(x)$ are divergent at the origin. The wavefunction must also vanish for all $\rho \geq R$, which establishes the allowed values of k;

$$k_m^n = \frac{\alpha_m^n}{R}; \quad n \in \{1, 2, 3, \dots\} \tag{2.22}$$

where α_m^n is the n^{th} zero of the Bessel function of order m. I have already established the allowed values of m in the radial part of the Schrödinger equation. The normalization condition gives me the value of the constant multiplier;

$$\psi_\rho = \frac{\sqrt{2}}{R} \frac{1}{|J_{m+1}(\alpha_m^n)|} J_m(k_m^n \rho), \tag{2.23}$$

and the energy of the state $|n, m\rangle$ is

$$E_{nm} = (k_m^n)^2 = \left(\frac{\alpha_m^n}{R}\right)^2. \tag{2.24}$$

To summarize, I have wavefunctions

$$\psi_{nm\ell}(\mathbf{r}) = \langle \mathbf{r} | nm\ell \rangle = \frac{\sqrt{2}}{R} \frac{1}{|J_{m+1}^2(\alpha_m^n)|} J_m(k_m^n \rho) \frac{1}{\sqrt{2\pi}} e^{im\phi} \sqrt{\frac{2}{L}} \sin\left(\frac{\ell \pi z}{L}\right) \tag{2.25}$$

with energies

$$E_{nm\ell} = \left(\frac{\alpha_m^n}{R}\right)^2 + \frac{\ell^2 \pi^2}{L^2}. \tag{2.26}$$

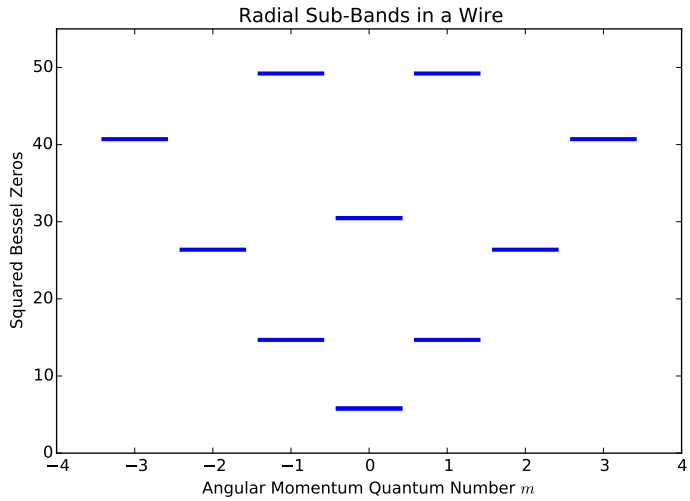

Figure 2.2: Ladder of radial sub-band states $(\alpha_m^n)^2$; *c.f.* the harmonic oscillator; Figure 1.1. The shells are enumerated in the same way (*spdf*), but note that the *d*- and *f*-shells are not fully degenerate here. In general, the only degeneracies are between levels of $\pm m$. The shell analogy is no longer a good one further up the ladder but suffices here.

2.2.1 Specifics of Quantum Wires

In a disk-shaped quantum dot, typically $L \lesssim R$, which leads to the energy spectrum being well-discretized. In a quantum wire, however, typically $L >> R$; effectively $L \to \infty$. This leads to a large number of levels increasing in ℓ at a given n and m.

The energy spectrum is thus characterized by *radial sub-bands*. The squared zeros of the Bessel function create a ladder of states $|n, m\rangle$. The structure is shown in Figure 2.2.

In a quantum wire of infinite length, the density of ℓ modes is proportional to $E^{-1/2}$ (Figure 2.3). It diverges near $\ell = 1$; at the edge of each radial sub-band. In real wires, with finite L, there is a quasicontinuum of levels within each radial sub-band.

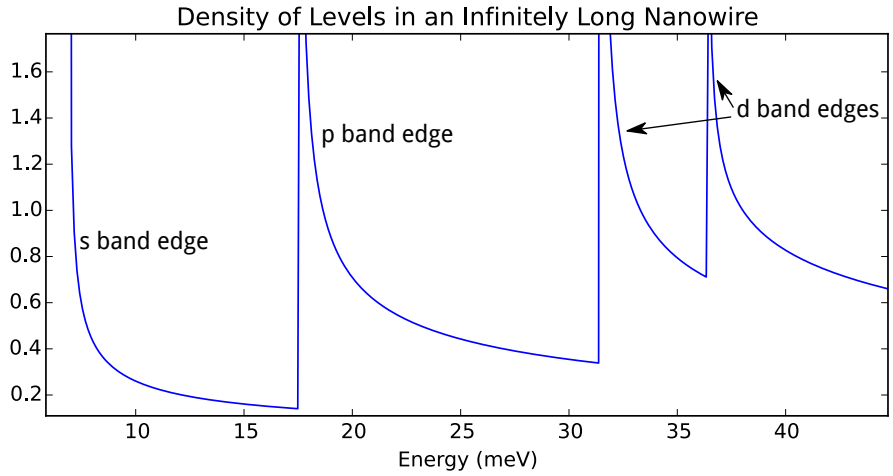

Figure 2.3: Density of levels in an infinitely long wire. The density is divergent near $\ell = 1$, in other words, near the radial sub-band edges $|n, m, 1\rangle$.

2.3 Single Quantum Dot Embedded in a Nanowire

I now have fully-characterized single-particle levels for a particle in a cylinder in the basis of Bessel node, angular momentum, and axial quantum numbers $\{n, m, \ell\}$.

While I could provide an "analytic" solution to the dot-in-a-wire problem based on boundary conditions for the potential, such a treatment is cumbersome and having explicit, closed-form wavefunctions provides little benefit when I will have to compute Coulomb matrix elements discretely anyway. Better, I can use the $\{n, m, \ell\}$ states to represent an empty quantum wire, but I am interested primarily in wires with embedded quantum dots. I treat this as a potential minimum within the wire; it has a radius $a \leq R$ and a height $2h << L$. If the dot is centered on the wire's axis, the potential is again independent of ϕ and the Hamiltonian is given by

$$H = H_0 + V_d(\rho, z), \tag{2.27}$$

where H_0 is the same Hamiltonian as (2.8) and

$$V_d(\rho, z) = \begin{cases} -V, & \left(\frac{L}{2} - h\right) \leq z \leq \left(\frac{L}{2} + h\right) \text{ and } 0 < \rho < a; \\ 0, & \text{otherwise;} \end{cases} \tag{2.28}$$

this is illustrated in Figure 2.4.

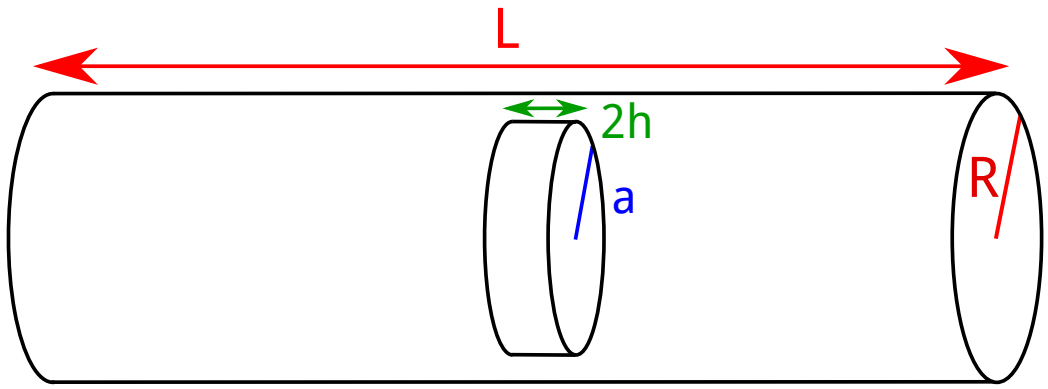

Figure 2.4: Illustration of a quantum wire with an embedded dot centered on $L/2$.

I can take the matrix element between two wire states:

$$\langle n_i m_i \ell_i | H_0 + V_d | n_j m_j \ell_j \rangle = E_i \delta_{ij} + \langle n_i m_i \ell_i | V_d | n_j m_j \ell_j \rangle \,. \tag{2.29}$$

As the $|n_i m_i \ell_i\rangle$ are precisely the eigenstates of H_0, with known eigenvalues, I can simply construct the Hamiltonian in the basis of $|n_i m_i \ell_i\rangle$, and diagonalize to obtain eigenfunctions of the form

$$\sum_i a_i \, |n_i m_i \ell_i\rangle \,. \tag{2.30}$$

The potential is not diagonal in the $|n_i m_i \ell_i\rangle$ basis. Its matrix element takes a value of

$$\begin{aligned} \langle n_i m_i \ell_i | V_d | n_j m_j \ell_j \rangle =& N_i N_j \; 2\pi \delta_{m_i m_j} \int_{\frac{L}{2}-h}^{\frac{L}{2}+h} dz \sin\left(\frac{\ell_i \pi z}{L}\right) \sin\left(\frac{\ell_j \pi z}{L}\right) \\ & \times \int_0^a \rho \, d\rho \, J_{m_i}(k_{m_i}^{n_i} \rho) J_{m_j}(k_{m_j}^{n_j} \rho), \end{aligned} \tag{2.31}$$

Where N_i is the full normalization constant for eigenfunction $\langle \mathbf{r} | \, n_i m_i \ell_i \rangle$. This integral will be needed again in the double dot with different limits. It is simpler to evaluate the indefinite integral at the limits whenever needed, rather than hard-code the definite integral of a particular system. There are cases, for example, where it is useful to not have the dot centered on $L/2$, though doing so preserves the symmetry

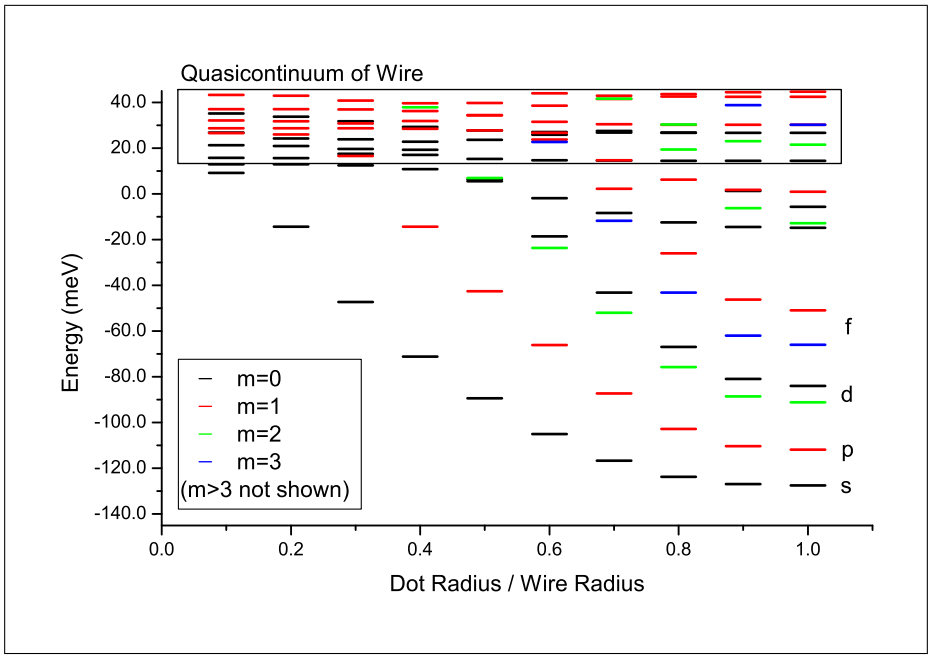

Figure 2.5: Growing a dot radially, at constant height. As the dot becomes similar in radius to the wire, the familiar *spd*-structure emerges. For each m except $m = 0$, there is a degenerate level at $-m$. The quasicontinuum boundary is the radial energy of the s-like (lowest energy) state in the empty wire.

of the wavefunction about that point of the solution. The indefinite integrals are

$$\int dz \sin\left(\frac{\ell_1 \pi z}{L}\right) \sin\left(\frac{\ell_2 \pi z}{L}\right) = \begin{cases} \frac{z}{2} - \frac{L}{4\pi\ell_1} \sin\left(\frac{2\ell_1 \pi z}{L}\right) & , \quad \ell_1 = \ell_2; \\ \frac{L}{2\pi}\left[\frac{1}{\ell_1-\ell_2} \sin\left(\frac{\pi(\ell_1-\ell_2)z}{L}\right) - \frac{1}{\ell_1+\ell_2} \sin\left(\frac{\pi(\ell_1+\ell_2)z}{L}\right)\right] & , \quad \ell_1 \neq \ell_2, \end{cases} \tag{2.32}$$

and

$$\int \rho\, d\rho\, J_m(k_1\rho) J_m(k_2\rho) = \begin{cases} \frac{1}{2}\rho^2 \left[J_m^2(k_1\rho) - J_{m-1}(k_1\rho) J_{m+1}(k_1\rho)\right] & , \quad n_1 = n_2; \\ \frac{\rho}{k_1^2-k_2^2}\left[k_2 J_{m-1}(k_2\rho) J_m(k_1\rho) - k_1 J_{m-1}(k_1\rho) J_m(k_2\rho)\right] & , \quad n_1 \neq n_2. \end{cases} \tag{2.33}$$

Having this result, I can now construct the Hamiltonian in the basis of $\{n, m, \ell\}$, and diagonalize it, to obtain the new eigenvalues and eigenstates. However, $\{n, m, \ell\}$

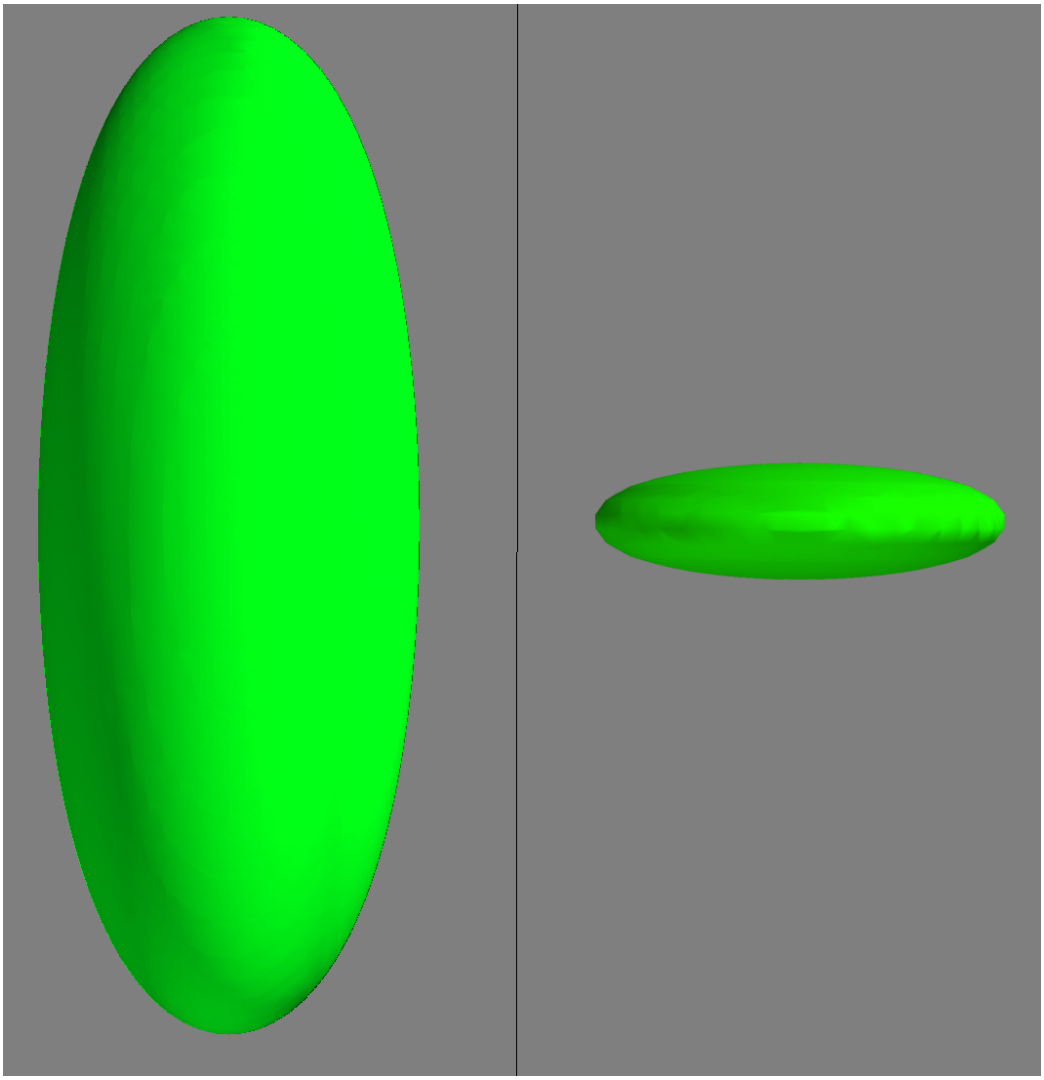

Figure 2.6: Isosurface comparison of the empty wire (left) to that of the same wire with an embedded dot (left). The scale is roughly the same in both.

is infinite-dimensional. I instead consider a truncated Hilbert space,

$$\{n, m, \ell \mid n < N, \ell < \Lambda\} \tag{2.34}$$

for suitably large N and Λ as determined by convergence tests. For the lowest eigenvalues the contribution from very high n, ℓ will vanish asymptotically. The rate of convergence also depends on the height of the dot relative to the length of the wire; very small dots in very long wires will converge much less rapidly. There is then a tradeoff between capturing the essence of an infinitely long wire while saving computation in the form of smaller eigenvalues.

Previously, for a very long wire ($L >> R \gtrsim a_B$), I had a quasicontinuum of states within each radial sub-band. In this system, however, a subset of states are confined to the dot, and these confined states do not exhibit a quasicontinuum. If h is sufficiently smaller than a, I recover the ordering and qualitative appearance of the spectrum of the infinite disk; namely a very similar s-, p-, and d-shell character (Figure 2.5).

We can also verify that these states are indeed confined. For a wire of length L unchanged, the fundamental wire mode $|1, 0, 1\rangle$ and the fundamental state confined to a dot are compared in Figure 2.6.

2.4 Vertically-Coupled Double Quantum Dot

Levels for a single dot are helpful, but the purpose of this thesis is to characterize an array of dots in a nanowire. Namely, I would like to determine the behaviour of two or more dots. Continuing to compute the interaction between $4N$ electrons over single-particle levels of an N-dot array quickly becomes intractable, but for the case of 2 dots I am able to perform all the same calculations as in the single-dot case. As such, I will determine single-particle levels for a two-dot system from the lowest-level treatment I have considered; namely, the effective mass approximation. This will help parameterize the spin-1 Heisenberg Hamiltonian and determine the J thereof.

I proceed in exactly the same way with the double-dot system as I did in Section

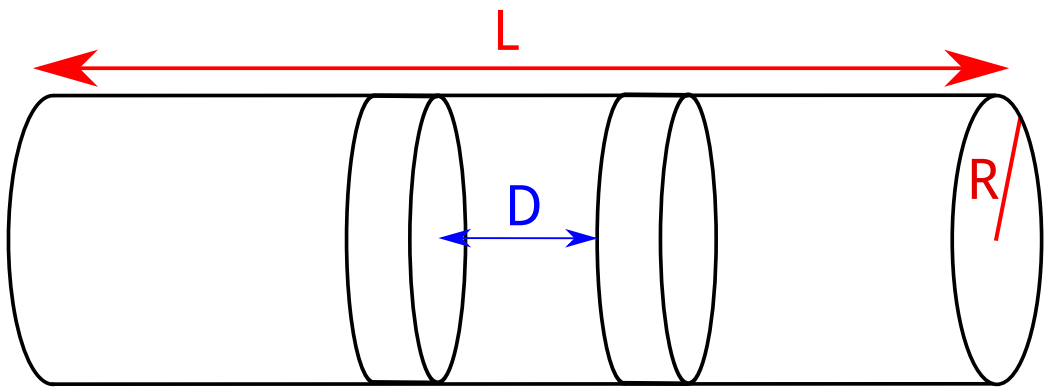

Figure 2.7: Illustration of a quantum wire with two dots of height h (note: the single dot had a height of $2h$) and radius equal to that of the wire. They are separated by D, which will become an important parameter.

2.3; by expanding in $|nm\ell\rangle$. In particular, I again can write

$$H = H_0 + V_{dd}(\rho, z), \tag{2.35}$$

and the only thing that has changed from before are the limits of the potential, which now depends on dot separation D as well as h and L;

$$V_{dd}(\rho, z) = \begin{cases} -V, & \left(\frac{L-D}{2} - h\right) \leq z \leq \left(\frac{L-D}{2}\right) \text{ and } 0 < \rho < a; \\ -V, & \left(\frac{L+D}{2}\right) \leq z \leq \left(\frac{L+D}{2} + h\right) \text{ and } 0 < \rho < a; \\ 0, & \text{otherwise.} \end{cases} \tag{2.36}$$

Here h is the thickness of the dots; whereas in the single dot I called the thickness $2h$. This is so that this model reduces exactly to a single dot when $D = 0$. This just gives me different limits of integration in (2.31) (indeed, I have to integrate once for each dot), for which I already have the indefinite integral. I proceed in exactly the same way as before; truncating my basis to N radial and Λ axial quantum numbers as determined by convergence tests.

While I need not restrict myself to cases where $a = R$, in doing so I lose very little generality in terms of the defining characteristics of my solution (as can be seen for the single dot), but gain quite a bit of simplicity computationally, as n becomes again a good quantum number. The dots are coupled vertically; the in-plane form of the wavefunction does not play a particularly important role, at least for identical

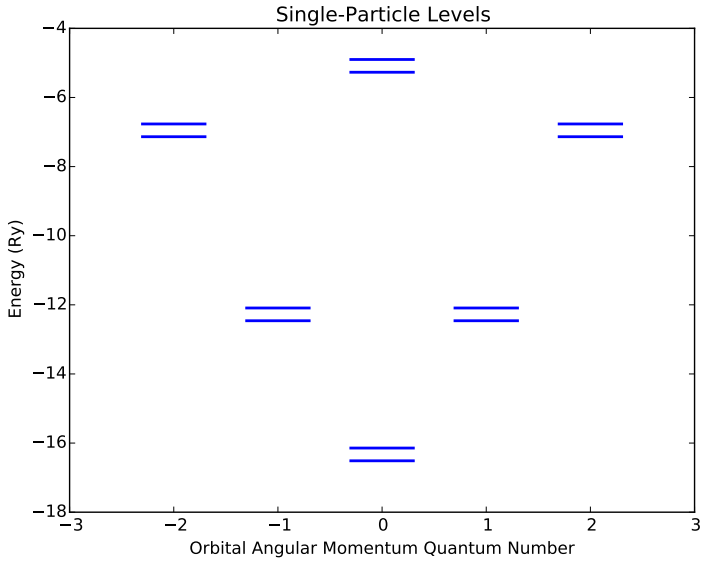

Figure 2.8: Single-particle levels of a particular 2-dot system ($h = 4$ nm and $D = 11$ nm), showing the s-, p-, and d-shells. In this regime the symmetric and antisymmetric levels are close together on the scale of the radial spacing. The splitting decreases with D, becoming zero in the infinite limit.

dots. I will also consider that the dots each have height h (previously it was one dot of height $2h$) to allow this two-dot system to reduce exactly to the one-dot potential when $D = 0$.

This system differs from the single dot in that each radial level splits (Figure 2.8). the splitting depends on dot separation, and is due to the symmetry of the wavefunction with respect to the two dots. The symmetric states $|n, m, S\rangle$ are lower in energy, as the probability density of the antisymmetric states $|n, m, AS\rangle$ vanish at $L/2$ (Figure 2.9).

This has important consequences when considering dot separation. It is helpful to consider the limits. Very well-separated dots ($D \to \infty$) will not interact. The wavefunction does not overlap between the dots, so the probability density of both $|S\rangle$ and $|AS\rangle$ go to 0 at $L/2$ anyway; they are indistinguishable from a probability density point of view. As such, the spectrum looks the same as the single dot, except that each level is twice degenerate. Very close dots $D \to 0$ will behave much like a

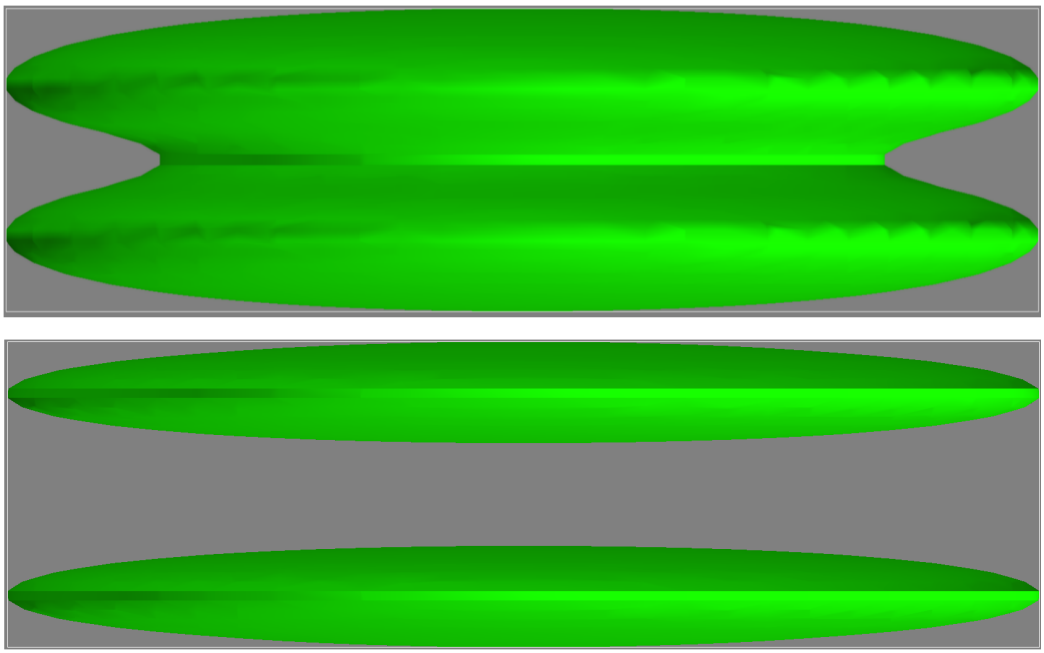

Figure 2.9: Isosurfaces of the probability density of s-type symmetric (top) and antisymmetric (bottom) wavefunctions. The antisymmetric wavefunction vanishes at $L/2$ (vertical center of the images) while the symmetric state overlaps. The dots are very close together ($D = 2h$) to better illustrate the difference.

single quantum dot with height $2h$ (that is, setting $D = 0$ exactly recovers the one-dot spectrum, as it must). In this case, the antisymmetric excited state will simply be the first excited state of a single dot (provided such a confined state exists) which is of course also antisymmetric (analogous to $\ell = 2$ in the infinite disk). Then, the maximum splitting between E_S and E_{AS} is the splitting between the two lowest states of a single dot with height $2h$.

I want the dots to be interacting, but I want the splitting between symmetric and antisymmetric levels to be small on the scale of the s-p splitting, for reasons that will become apparent when I let electrons interact in the system.

2.5 The Tight-Binding Method

An alternative method of calculating the wavefunctions for the two-dot system is to treat the two dots separately, and hybridize their orbitals. This is completely analogous to the linear combination of atomic orbitals (LCAO) method used in quantum chemistry, however here the orbitals are cylindrical eigenfunctions. This method is routinely used in the computation of itinerant orbitals in lateral quantum-dot molecules[5][19][20].

The purpose of my inclusion of this method is that it gives direct insight into the nature of the splitting between the symmetric and antisymmetric levels in a two-dot system (and, more generally, the itinerant orbitals of a multi-dot system); they are given as exact combinations of single-dot orbitals. This method is an illustrative one in this sense; it provides an exact solution to compare with the numerics. It is also conceptually easier to think of the interaction between electrons on two dots and the hopping between them than delocalized electrons simultaneously occupying both dots.

I start with a basis of one orbital on each site; denoted "left dot" and "right dot" $|L\rangle$ and $|R\rangle$, respectively, with a given n, m (in a system with $a = R$). This is not a complete basis of my system, but it will do well as an approximation given that the parameters of my systems have been chosen so that only a single axial level is confined given n, m. The tight-binding method is exact only insofar as every possible orbital is taken into account.

I am looking to recover approximations to two vertical eigenstates, namely $|S\rangle$ and $|AS\rangle$. My Hamiltonian is

$$H = -\nabla^2 + V_\rho(\rho) + V_L(z) + V_R(z), \tag{2.37}$$

with the usual V_ρ, but V_L and V_R are the potentials for the left and right dot, respectively. I will assume their midpoint is centered on $L/2$ and that they are identical, as in the previous section. Obviously $|L\rangle$ and $|R\rangle$ do not diagonalize this Hamiltonian. In fact they are not even orthogonal, so I must cast this as a *generalized eigenvalue problem* in this basis $\{|L\rangle, |R\rangle\}$.

I begin by writing the Schrödinger equation expanded in this basis;

$$H \sum_{i=L,R} A_i \left|i\right\rangle = E \sum_{i=L,R} A_i \left|i\right\rangle, \tag{2.38}$$

Where A_i are the expansion coefficients. Multiplying on the left of both sides by another state $\langle j|$, this becomes

$$\sum_{i=L,R} \langle j|H|i\rangle \, A_i = E \sum_{i=L,R} \langle j|\, i\rangle \, A_i. \tag{2.39}$$

Defining $H_{tb}^{ji} = \langle j|H|i\rangle$ and $S_{tb}^{ji} = \langle j|\, i\rangle$, this can be cast into a generalized eigenvector problem for the vector $\boldsymbol{A}$ of coefficients A_i that diagonalize the Hamiltonian;

$$\hat{H}_{tb}\boldsymbol{A} = E\hat{S}_{tb}\boldsymbol{A}. \tag{2.40}$$

In an orthogonal basis S_{tb} is the identity matrix, reducing the problem to a standard eigenvalue problem. The quantity $s \equiv \langle L|\, R\rangle$ is the overlap integral of the two wavefunctions,

$$s = \int_0^L dz \; \psi_L^*(z)\psi_R(z); \tag{2.41}$$

The overlap matrix is then

$$\hat{S}_{tb} = \begin{pmatrix} 1 & s \\ s & 1 \end{pmatrix}, \tag{2.42}$$

where s is strictly less than unity, and typically very small (hence the "tight-binding" of the orbitals to their dots).

This can be transformed into a standard eigenvalue problem, with different eigenvectors, by defining $\boldsymbol{B} = \hat{S}_{tb}^{1/2}\boldsymbol{A}$ and then rewriting Equation (2.40) as

$$\hat{S}_{tb}^{-1/2}\hat{H}_{tb}\hat{S}_{tb}^{-1/2}\boldsymbol{B} = E\boldsymbol{B}. \tag{2.43}$$

The square root of a diagonalizable matrix M is

$$M^{1/2} = P^\dagger D^{1/2} P, \tag{2.44}$$

where D is the diagonal form of M with corresponding eigenvectors forming the columns of P. $D^{1/2}$ has as entries the square root of the entries in D. For the matrix

S_{tb} with eigenvalues $1 \pm s$, this amounts to

$$S_{tb}^{1/2} = \frac{1}{2}\begin{pmatrix} \sqrt{1+s}+\sqrt{1-s} & \sqrt{1+s}-\sqrt{1-s} \\ \sqrt{1+s}-\sqrt{1-s} & \sqrt{1+s}+\sqrt{1-s} \end{pmatrix} \tag{2.45}$$

and so

$$S_{tb}^{-1/2} = \frac{1}{2\sqrt{1-s^2}}\begin{pmatrix} \sqrt{1+s}+\sqrt{1-s} & \sqrt{1-s}-\sqrt{1+s} \\ \sqrt{1-s}-\sqrt{1+s} & \sqrt{1+s}+\sqrt{1-s} \end{pmatrix}. \tag{2.46}$$

Now I must work out the components of H_{tb}. I can write

$$H_{tb} = H_L + V_R(z), \tag{2.47}$$

where $|L\rangle$ is an eigenfunction of H_L (for which I have already solved), and where there is a completely analogous representation favouring the right dot.

The off-diagonal matrix element of H_{tb}, which I denote the "tunneling" matrix element $-t$ is

$$-t \equiv \langle R|H_{tb}|L\rangle = E_L \langle R|L\rangle + \langle R|V_R|L\rangle . \tag{2.48}$$

I have written $-t$ presupposing its negative value, which will tend to be the case.

The diagonal terms are likewise

$$E_0 \equiv \langle L|H|L\rangle = E_L + \langle L|V_R|L\rangle , \tag{2.49a}$$

$$E_0 \equiv \langle R|H|R\rangle = E_R + \langle R|V_L|R\rangle ; \tag{2.49b}$$

which are identical due to symmetry. I will rescale to $E_0 = 0$ for convenience.

The tight-binding Hamiltonian is then

$$H_{tb} = \begin{pmatrix} 0 & -t \\ -t & 0 \end{pmatrix} \tag{2.50}$$

and so

$$S_{tb}^{-1/2} H S_{tb}^{-1/2} = \frac{t}{1-s^2}\begin{pmatrix} s & -1 \\ -1 & s \end{pmatrix}. \tag{2.51}$$

The vectors $\boldsymbol{B}$ are then

$$\frac{1}{\sqrt{2}}(|L\rangle + |R\rangle) \tag{2.52a}$$

$$\frac{1}{\sqrt{2}}(-|L\rangle + |R\rangle) \tag{2.52b}$$

Which give the corresponding $\boldsymbol{A} = S_{tb}^{-1/2}\boldsymbol{B}$ as

$$\frac{1}{\sqrt{2(1+s)}}(|L\rangle + |R\rangle) \tag{2.53a}$$

$$\frac{1}{\sqrt{2(1-s)}}(-|L\rangle + |R\rangle) \tag{2.53b}$$

with eigenvalues $-t/(1+s)$ and $t/(1-s)$, respectively (recall that I rescaled to $E_0 = 0$). One can easily verify that they are normalized. The splitting is hence $2t/(1-s^2)$; approximately $2t$ to second order in s.

Again, this treatment is useful because it gives a more intuitive understanding of the splitting of radial sub-bands. By treating each dot separately, we see the emergence of equally-weighted hybridizations of their orbitals (as we must due to the symmetry of the problem); which is perhaps somewhat obfuscated in the brute-force diagonalization including the two potentials together.

I will now occasionally refer to the symmetric-antisymmetric splitting of the two dots as $2t$ (neglecting the small $1 - s^2$), especially in extensions to the tight-binding model.

Chapter 3

Interacting Systems of Electrons

I now have single-particle levels for my quantum dot systems; these are important in further calculations involving systems of several electrons, with which I proceed presently. I will now move to loading these systems with electrons and solving the interacting Hamiltonian. It is convenient to express this problem in the language of second-quantization; in this formalism an N-particle state is represented by particle creation operators $c^+_{i\sigma}$ for single-particle state i with spin $\sigma \in \{\uparrow, \downarrow\}$ acting on the vacuum (zero-particle) state $|0\rangle$ as such:

$$c^+_{i_1\sigma_1} c^+_{i_2\sigma_2} \cdot \ldots \cdot c^+_{i_N\sigma_N} |0\rangle \,. \tag{3.1}$$

I will further introduce its Hermitian conjugate, the annihilation operator $c_{i\sigma}$, whose action on a state is to remove an electron with i, σ:

$$c_{i\sigma} c^+_{i\sigma} |0\rangle = |0\rangle \tag{3.2}$$

All of the consequences of fermionic statistics are contained in the anticommutation relations

$$\{c^+_{i\sigma}, c^+_{j\sigma'}\} = 0; \tag{3.3a}$$

$$\{c_{i\sigma}, c_{j\sigma'}\} = 0; \tag{3.3b}$$

$$\{c_{i\sigma}, c^+_{j\sigma'}\} = \delta_{ij}\delta_{\sigma\sigma'}; \tag{3.3c}$$

namely, (3.3a) guarantees that permuting two operators introduces an overall negative sign (and hence preserves the antisymmetry of the fermions), as well as guaranteeing that creating two electrons on the same state results in 0 (preserving Pauli exclusion). In this way, a product of creation operators acting on $|0\rangle$ is a convenient notation for a Slater determinant over the states they represent.

In this formalism, the N-particle Hamiltonian is

$$H = \sum_i \sum_\sigma c^+_{i\sigma} c_{i\sigma} E_i + \frac{1}{2} \sum_{ijkl} \sum_{\sigma\sigma'} c^+_{i\sigma} c^+_{j\sigma'} c_{k\sigma'} c_{l\sigma} \langle ij|V|kl\rangle \tag{3.4}$$

where the first term counts particles in a single-particle level, and the second term is the two-particle Coulomb term between initial state with electrons on levels i and j and final state with electrons on l and k.The term containins the Coulomb matrix element between the two two-particle configurations, expressed in the position basis:

$$\langle ij|V|kl\rangle = 2 \int_{\mathbb{R}^3} d^3 r_1 \int_{\mathbb{R}^3} d^3 r_2 \, \frac{\langle i|\,\mathbf{r}_1\rangle \, \langle j|\,\mathbf{r}_2\rangle \, \langle \mathbf{r}_2|\,k\rangle \, \langle \mathbf{r}_1|\,l\rangle}{|\mathbf{r}_1 - \mathbf{r}_2|} \tag{3.5}$$

where I have implicitly accounted for the fact that each particle's spin is a good quantum number with respect to the Coulomb potential.

One can see that for the Coulomb term between two configurations to be nonzero, the configurations must have their electrons loaded onto all of the same single-particle levels (with the same spin) up to two or fewer differences, for if they differ by more than two operators, the term

$$\left\langle 0 \middle| c_{i_1\sigma_1} \cdot \cdots \cdot c_{i_N\sigma_N} \; c^+_i c^+_j c_k c_l \; c^+_{i_{N+1}\sigma_{N+1}} \cdot \cdots \cdot c^+_{i_{2N}\sigma_{2_N}} \middle| 0 \right\rangle \tag{3.6}$$

will be zero for any combination of $ijkl$ by orthogonality.

3.1 Coulomb Matrix Elements

In some cases, such as the Harmonic oscillator, the Coulomb matrix elements (3.5) can be computed analytically[27]. Outside of a few simple systems no closed form solution is known, and so in general one must compute Coulomb matrix elements numerically. To this end I use a discretized 3D integration, as, for example, in ref. [28].

I approximate the two-particle integral by discretizing space, treating my $\psi_\alpha(\mathbf{r})$ over the normally continuous variable $\mathbf{r}$ as existing only on lattice points $\mathbf{R}$; that is,

$$\psi_i(\mathbf{r}) \approx \psi_i(\mathbf{R}). \tag{3.7}$$

The differentials dx^j (the usual Cartesian $\{x^j\}$) are now finite;

$$dx\,dy\,dz \approx \Delta x_i \Delta y_i \Delta z_i = \Delta V_i. \tag{3.8}$$

The integrals become sums over discrete sites, and if the spacing between lattice points and hence ΔV_i are taken to be identical for every cell, this is

$$\int_{\mathbb{R}^3} d^3r \approx \sum_{\mathbf{R}} \Delta V. \tag{3.9}$$

This changes the normalization condition for a wavefunction to

$$\sum_{\mathbf{R}} \Delta V \left|\psi(\mathbf{R})\right|^2 = 1. \tag{3.10}$$

The Coulomb matrix element is then

$$\langle ij|V|kl\rangle = (\Delta V)^2 \sum_{\mathbf{R_1},\mathbf{R_2}} \psi_i^*(\mathbf{R}_1)\psi_l(\mathbf{R}_1)\frac{2}{|\mathbf{R}_1-\mathbf{R}_2|}\psi_j^*(\mathbf{R}_2)\psi_k(\mathbf{R}_2). \tag{3.11}$$

This can be written as a matrix multiplication, more clearly by writing composite indices $\{il\},\{jk\} = \alpha,\beta$:

$$V_{\alpha,\beta} = \Phi^T_{\alpha,\mathbf{R}_1} U_{\mathbf{R}_1,\mathbf{R}_2} \Phi_{\mathbf{R}_2,\beta}, \tag{3.12}$$

where summation over repeated indices is assumed. $\Phi_{\mathbf{R}_2,\beta}$ is a matrix containing (column-wise) possible products $\psi_j^*\psi_k$ evaluated (row-wise) on all lattice points $\mathbf{R}_2$. Namely, if there are N lattice points and M eigenstates, this matrix is $N \times M^2$. $U_{\mathbf{R}_1,\mathbf{R}_2}$ is the Coulomb term between latice sites $\mathbf{R}_1$ and $\mathbf{R}_2$;

$$U_{\mathbf{R}_1,\mathbf{R}_2} = \frac{2}{|\mathbf{R}_1-\mathbf{R}_2|}. \tag{3.13}$$

and is $N \times N$. N is typically as large as possible ($N > 10^6$), so this is computed on the fly. For diagonal terms I introduce a small separation ϵ such that

$$U_{\mathbf{R},\mathbf{R}} = \frac{2}{\epsilon}, \tag{3.14}$$

which is fitted for a particular lattice against a known matrix element.

The result of this matrix product, $V_{\alpha,\beta}$ is an $M^2 \times M^2$ matrix containing all the desired Coulomb matrix elements.

3.2 The Configuration-Interaction Method

Now that I am able to compute Coulomb matrix elements, I can proceed to solve the interacting Hamiltonian (3.4) via the *configuration-interaction* (CI) method. This treatment is an exact diagonalization of the interacting Hamiltonian if every confined single particle level of the quantum dot is included. I will always limit my consideration to a subset of these; first the p-shell, and then a verification of the results with the s-, p- and d-shells. For a system with N single-particle levels and k electrons, there are

$$\left(\begin{array}{c} 2N \\ k \end{array} \right), \tag{3.15}$$

configurations, growing factorially in N and quickly rendering computation intractable. This can be reduced by total spin; if $k_\uparrow$ of the k electrons are spin-up, there are

$$\left(\begin{array}{c} N \\ k_\uparrow \end{array} \right) \left(\begin{array}{c} N \\ k - k_\uparrow \end{array} \right) \tag{3.16}$$

configurations with spin $k_\uparrow - k_\downarrow$, however this is of the same order of magnitude.

It will help to rewrite the Coulomb term of the Hamiltonian, first as

$$\frac{1}{2} \sum_{ijkl} c_i^+ c_j^+ c_k c_l \left\langle ij|V|kl \right\rangle , \tag{3.17}$$

where $ijkl$ are composite indices indicating state *and* spin. I now have to explicitly include the fact that spin must be preserved by V, but I gain a nice simplification. I proceed to write (3.17) in a form that does not double-count terms. Specifically, for every ij, kl it is clear from (3.5) that ji, lk is identical. I can separate the sum into two parts. Assuming that I have in some way consistently ordered my states; for example, such that the lowest-lying electrons appear leftmost (rightmost) in a product of creation (annihilation) operators, this will be more convenient. Let us assume that I have chosen this convention. Regardless, I can write

$$\frac{1}{2} \left(\sum_{ij,\ k>l} c_i^+ c_j^+ c_k c_l \left\langle ij|V|kl \right\rangle + \sum_{ij,\ k<l} c_i^+ c_j^+ c_k c_l \left\langle ij|V|kl \right\rangle \right) \tag{3.18}$$

and then in the second term permute c_k^+ and c_l^+ (introducing a negative sign), and swap the dummy indices k and l; this leaves

$$\frac{1}{2}\sum_{ij,\, k>l} c_i^+ c_j^+ c_k c_l \left(\langle ij|V|kl\rangle - \langle ij|V|lk\rangle\right). \tag{3.19}$$

Performing the same manipulation on indices i and j gives me the same two terms, in this way I lose the factor of $1/2$;

$$\sum_{i<j,\, k>l} c_i^+ c_j^+ c_k c_l \left(\langle ij|V|kl\rangle - \langle ij|V|lk\rangle\right), \tag{3.20}$$

as well as the need to keep track of half of the nonzero terms in a matrix element. Further, this restriction introduces the nice property that i, l will always operate on electrons that are created further from $\langle 0|$ and $|0\rangle$ in the product than j, k, greatly simplifying the permutation algebra needed.

3.2.1 Two Interacting Electrons on a p-Shell

To demonstrate the configuration interaction method, I will present a full solution for the interaction of two electrons on a p-shell. Recall that the p-shell is doubly degenerate; both states have energy E_p and have orbital angular momentum $L \equiv m = \pm 1$. Total L is conserved by the Coulomb interaction, as is total S_z. S^2 is a good quantum number, but it is not diagonal in configurations. I can then, upon diagonalizing, express my results in the basis

$$\{|L, S, S_z\rangle\}, \tag{3.21}$$

where the eigenvalue of S^2 is $S(S+1)$. I can for now reduce my basis of configurations into sub-bases with fixed L and S_z; it turns out that for this system only one such sub-basis has more than one element; namely $S_z = L = 0$ has two elements.

I will label the single-particle levels $m = -1, 1$ as $1, 2$, respectively, for notational convenience. The $S_z = L = 0$ sub-basis is $\{c_{1\uparrow}^+ c_{2\downarrow}^+ |0\rangle, c_{1\downarrow}^+ c_{2\uparrow}^+ |0\rangle\} \equiv \{|a\rangle, |b\rangle\}$, illustrated schematically in Figure 3.1.

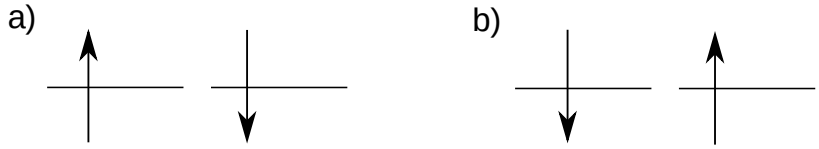

Figure 3.1: The degenerate p-shell is shown with $L = -1$ on the left and $L = 1$ on the right. a) Configuration $|a\rangle$. b) Configuration $|b\rangle$.

The diagonal elements of the Hamiltonian (3.4) contain two sets of terms; I will call them H_0 and V where brevity is needed. For the former,

$$\sum_i E_i \left\langle 0\middle|c_{2\downarrow}c_{1\uparrow}c_i^+c_ic_{1\uparrow}^+c_{2\downarrow}^+\middle|0\right\rangle, \tag{3.22}$$

The annihilation operator in the middle (c_i) acts to the right to annihilate an electron, as does the creation operator to the left (recall they are Hermitian conjugates). The final configuration of creation operators acting on $|0\rangle$ must be the same (in reverse order) as that of annihilation operators acting on $\langle 0|$. Hence, there are two surviving terms; $i = 1\uparrow$ and $i = 2\downarrow$. For the latter, I need to make two operator permutations to recover terms of the form (3.2); as this is an even number the overall phase is positive and I am left with $2E_p$; twice the energy of the p-shell orbitals.

For the potential term,

$$\left\langle 0\middle|c_{2\downarrow}c_{1\uparrow}\ V\ c_{1\uparrow}^+c_{2\downarrow}^+\middle|0\right\rangle, \tag{3.23}$$

from a brief analysis of (3.20), I find that I have exactly one nonzero choice of $ijkl$;

$$i = l = 1\uparrow; \tag{3.24a}$$

$$j = k = 2\downarrow. \tag{3.24b}$$

I am left with two terms; removing the spin components that are individually diagonal in V they are

$$\langle 12|V|21\rangle \langle\uparrow|\uparrow\rangle \langle\downarrow|\downarrow\rangle - \langle 12|V|12\rangle \langle\uparrow|\downarrow\rangle \langle\downarrow|\uparrow\rangle. \tag{3.25}$$

The second term vanishes because of the unlike spins. The contribution from V is then given solely by the term

$$\langle 12|V|21\rangle; \tag{3.26}$$

often referred to as the *direct* Coulomb matrix element (V_{dir}) between electrons on states 1 and 2.

It should go without saying that the diagonal terms are equal; in total I have

$$H_{aa} = H_{bb} = 2E_p + \langle 12|V|21\rangle \equiv E_0 \tag{3.27}$$

I now turn my attention to the off-diagonal. By construction H_0 is strictly diagonal so will not contribute anything here. Then,

$$H_{ab} = \left\langle 0\middle|c_{2\downarrow}c_{1\uparrow}\, V\, c^+_{1\downarrow}c^+_{2\uparrow}\middle|0\right\rangle \tag{3.28}$$

Here, the only possibility is

$$i = 1\uparrow; \tag{3.29a}$$

$$j = 2\downarrow; \tag{3.29b}$$

$$k = 2\uparrow; \tag{3.29c}$$

$$l = 1\downarrow, \tag{3.29d}$$

which leaves

$$\langle 12|V|21\rangle \langle\uparrow|\downarrow\rangle \langle\downarrow|\uparrow\rangle - \langle 12|V|12\rangle \langle\uparrow|\uparrow\rangle \langle\downarrow|\downarrow\rangle \tag{3.30}$$

In this case it is the first term that vanishes due to spin, leaving

$$H_{ab} = H_{ba} = -\langle 12|V|12\rangle; \tag{3.31}$$

which is often called the *exchange* Coulomb matrix element (V_{ex}) between states 1 and 2, and is always weaker than V_{dir}.

This Hamiltonian reduces to the simplest nontrivial one

$$H = \begin{pmatrix} E_0 & -V_{ex} \\ -V_{ex} & E_0 \end{pmatrix} \tag{3.32}$$

which has eigenvectors

$$|\pm\rangle = \sqrt{\frac{1}{2}}\left(|a\rangle \pm |b\rangle\right) \tag{3.33}$$

with energies

$$E_\pm = 2E_p + V_{dir} \mp V_{ex}. \tag{3.34}$$

I know these states have $S_z = 0$ and $L = 0$, and can determine S by comparison with the $S_z = 1, L = 0$ state, which will necessarily be degenerate with the state here with $S = 1$ since there is nothing in the Hamiltonian to favour (or even depend on at all) a particular S_z. Indeed, for the only possible $S_z = 1$ configuration,

$$c^+_{1\uparrow} c^+_{2\uparrow} |0\rangle \,, \tag{3.35}$$

I find the H_0 term is of course still $2E_p$, while the V term is the same as that in (3.25) save for all spins pointing in the same direction. Thus, the exchange term does not vanish and I am left with

$$E_{S_z=1} = 2E_p + V_{dir} - V_{ex}; \tag{3.36}$$

precisely the energy of $|+\rangle$. We can then identify $|+\rangle$ as the $S_z = 0$ component of the spin-triplet; $|L, S, S_z\rangle = |0, 1, 0\rangle$; this is the ground state of the system, separated from the singlet by $2V_{ex}$.

This property of spin projections allows me to determine S for any CI calculation I perform as well as easily check for a particular class of implementation error; if an energy level exists in the $S_z = N$ basis it had better exist in all other bases $-N \leq S_z < N$.

One can (trivially but somewhat tediously) explicitly write out the Slater determinants to verify that indeed I have generated the ($S_z = 0$) spin-singlet and spin-triplet states in the more familiar form

$$\frac{1}{\sqrt{2}} \left(|\uparrow\downarrow\rangle \pm |\downarrow\uparrow\rangle \right), \tag{3.37}$$

where I have disregarded the spatial part of the wavefunction.

I have presented here a very simple example of electrons interacting in a quantum dot, however it is a representative one; I will find in the next section that a spin-1 ground state is to be expected, and that a main factor is the exchange potential on the p-shell.

3.2.2 Single Quantum Dot with 4 Electrons

I move now to the treatment of a quantum dot with six levels (*spd*) and four electrons. The single-particle levels are those of Section 2.3; namely, the quantum dot embedded

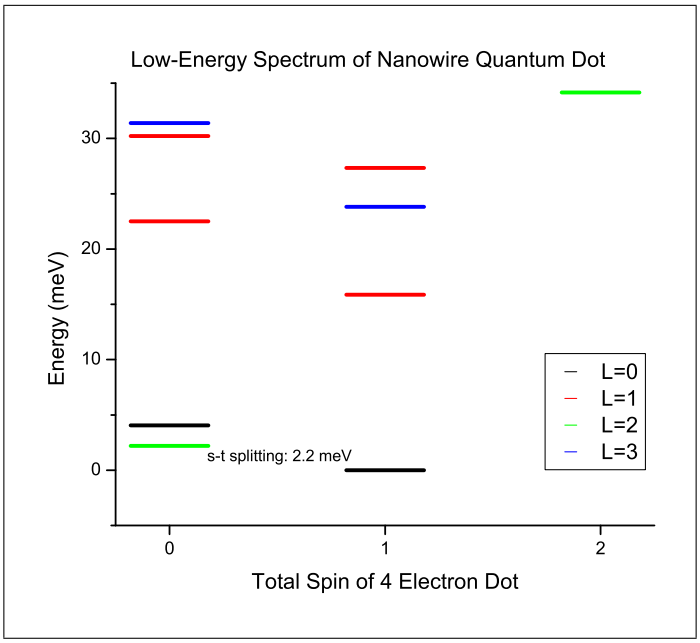

Figure 3.2: Several lowest energy levels of a nanowire quantum dot, with $R = a = 4$ nm and $2h = 4$ nm. The length of the wire plays no role when it is $\sim 5h$. The potential depth is 100 meV.

in a nanowire with $a = R$. There are a very manageable 495 total configurations; the largest spin sector which is always $S_z = 0$ has 225. I will be able to construct and diagonalize these matrices by conventional means (that is, using LAPACK).

The validity of the *spd* approximation is determined by the splitting between the shells. As the main effect is one that arises from the p-shell interaction with some admixture from higher excitations (recall that Hund's rules have been shown to hold in quantum dots), where the admixture is stronger if the states are close in energy compared to the strength of the Coulomb elements that mix them (which are also much larger in lower states, the s-level particularly, than in higher ones). Real quantum dots are of course not infinitely confining, and so do not actually exhibit infinitely many confined states. Indeed, I have specifically tuned parameters in my finite dots so that few higher excitations are confined. In any case, the decision to ignore excitations past the d-shell is not an arbitrary one[14].

The procedure is exactly the same as in Section 3.2.1, except that for both H_0 and

V terms there will be many more nonzero contributions to account for. The matrices will however be sparsely-populated due to the fact that the Coulomb interaction is a two-body potential; interacting configurations must be identical up to two electrons in order to have a nonzero matrix element.

The result of one such diagonalization is shown in Figure 3.2. Indeed a spin-1 ground state emerges in this particular 4-electron system. Of note is that the spin-triplet persists at the lowest energy across any 4-electron system I have looked at.

This is fundamentally the same result as the two electrons on a p-shell model, though the spectrum is of course more complex. Here there are 495 states, but the salient feature of the p-shell model and the desired outcome for realizing an antiferromagnetic spin chain was the spin-1 ground state, which persists including interactions with the s-shell and d-shell.

3.2.3 The Heisenberg Hamiltonian for Two Sites

I will make comparisons with the Heisenberg Hamiltonian for two sites soon so I will derive its solution here, with reference to [29] for operator definitions.

The atomic unit of the Heisenberg model is the spin product

$$\boldsymbol{S}_i \cdot \boldsymbol{S}_j. \tag{3.38}$$

It is helpful to make use of the spin-raising and -lowering operators

$$S_j^{\pm} = S_j^x \pm i S_j^y. \tag{3.39}$$

They act to raise (or lower) the z-component of a spin if a higher (or lower) polarity exists;

$$S^{\pm} \left|S, S_z\right\rangle = \sqrt{S(S+1) - S_z(S_z \pm 1)} \left|S, S_z \pm 1\right\rangle. \tag{3.40}$$

For $S = 1$, $S_z \in \{-1, 0, 1\}$, wherever I may increment or decrement the spin (obeying $-S_z < S < S_z$), I have

$$\sqrt{S(S+1) - S_z(S_z \pm 1)} = \sqrt{2}, \tag{3.41}$$

which is easy to see as in all cases the S_z part becomes 0.

In defining this I am free to rewrite the 2-spin Hamiltonian; it becomes

$$\frac{1}{2}(S_i^+ S_j^- + S_i^- S_j^+) + S_i^z S_j^z, \tag{3.42}$$

which immediately exposes the property that incrementing spin i must decrement spin j and vice-versa—The Hamiltonian conserves total S_z—as well as the fact that the increment/decrement terms are purely off-diagonal. Spin-polarizations are degenerate as always, which allows me to determine S of the eigenvalues without explicitly checking $\langle S^2 \rangle$.

Where it is ambiguous, $|0,0\rangle$ refers to $\left|S_i^z = 0, S_j^z = 0\right\rangle$; I will explicitly write $|S = 1, S_z = 0\rangle$ when using the total S^2 eigenbasis.

In the $S_z = 2$ (and equivalently -2) subset there is exactly one configuration, and it has energy 1;

$$S_i^z S_j^z \left|1,1\right\rangle = \left|1,1\right\rangle. \tag{3.43}$$

In the $S_z = 1$ basis (equivalently -1), there are two configurations, $\{|0,1\rangle, |1,0\rangle\}$, both with 0 energy, and in each, exactly one of the increment/decrement term acts in a nonzero manner, for example,

$$\frac{1}{2} S_1^+ S_2^- \left|0,1\right\rangle = \frac{\sqrt{2}\sqrt{2}}{2} \left|1,0\right\rangle = \left|1,0\right\rangle, \tag{3.44}$$

giving me the Hamiltonian

$$H_1 = \begin{pmatrix} 0 & 1 \\ 1 & 0 \end{pmatrix}, \tag{3.45}$$

which has eigenvalues ± 1, of which I already know which is $S = 2$ and so can deduce that the other is $S = 1$.

The $S_z = 0$ basis is $\{|-1,1\rangle |0,0\rangle |1,-1\rangle\}$; I won't go through it explicitly but the $|\pm 1, \mp 1\rangle$ states have energy -1 and connect only to $|0,0\rangle$; the Hamiltonian is

$$H_0 = \begin{pmatrix} -1 & 1 & 0 \\ 1 & 0 & 1 \\ 0 & 1 & -1 \end{pmatrix}, \tag{3.46}$$

which has eigenvalues $-2, -1, 1$. ± 1 are accounted for so -2 must be the singlet.

To summarize, the Heisenberg spectrum for two sites has a singlet ground state at $-2J$, a triplet at $-J$, and finally a quintuplet at J.

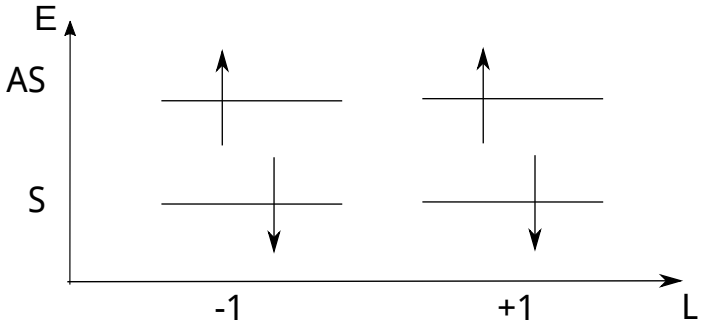

Figure 3.3: A sample configuration for the double-dot p-shell system. The energy levels may be doubly occupied as well.

3.2.4 Double Quantum Dot with 4 Electrons on the p-Shells

One might expect that since the ground state of a single quantum dot with 4 electrons is spin-1, then two such dots would interact like spin-1 objects, at least over an energy scale comparable to the excitation energy from this ground state. I of course need to verify this. A full 8-electron treatment of the two-dot system with 12 single-particle levels involves 735 471 configurations. As always I can partition this by spin, but the spin-0 sub-basis has 245 025 states; too large to store the matrix in full, let alone diagonalize conventionally. There is also the caveat that this is computationally quite costly. Computing Coulomb matrix elements takes a very long time, as does the construction of the interacting Hamiltonian, even with some optimization done.

Rather, it is helpful to consider a reduced basis at first to determine the range of parameters that might lead to suitable results in a full treatment. Much like in the single dot and for much the same reason, I will now consider interactions on the p-shells of a double-dot system. Recall this system has two p-shells; the symmetric and antisymmetric subshells. One can also imagine the p-shell of the left dot and p-shell of the right dot, as in the tight-binding treatment of Section 2.5.

Physically, the assumption is that 2 electrons are "frozen in" to the s-shell on both dots and do not contribute (*i.e.* they are core electrons), while the d-shell is inaccessibly high in energy. This can be achieved approximately in practice with proper tuning of the level spacing.

As the desired effect in a single dot was the result of two electrons interacting on

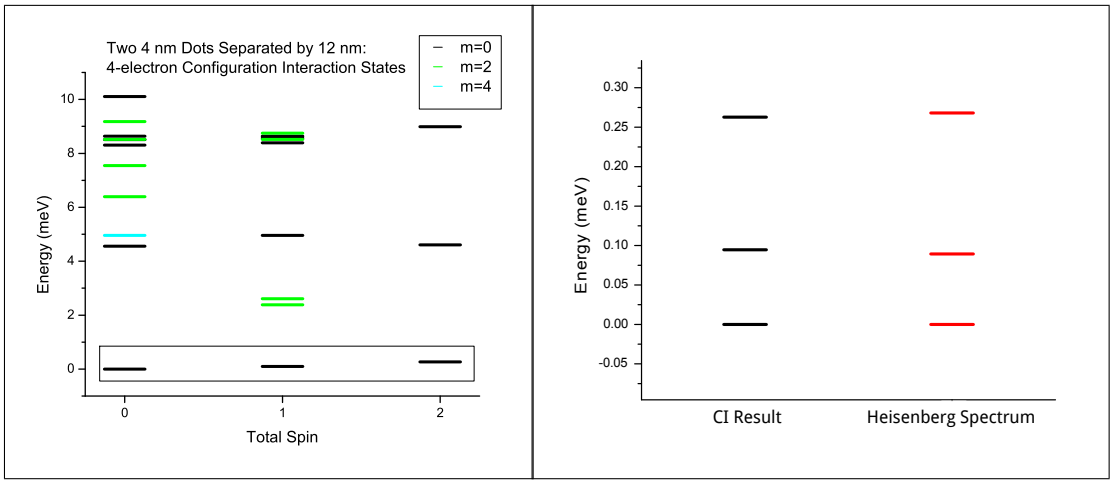

(a) (b)

Figure 3.4: Spectrum of a particular interacting p-shell system. $h = 4$ nm, $R = a = 18$ nm. The dots are separated by 12 nm. a) The full spectrum excluding one singlet state far above these. Degeneracies are not resolved. b) The boxed portion of the spectrum in a) showing excellent correspondence to the Heisenberg spectrum for spin-1 objects. In both cases the ground state is a spin-0 singlet, next bar is a spin-1 triplet, and the last bar a spin-2 quintuplet. The Heisenberg J was fitted against the average of the two splittings in the CI result, and both spectra are scaled to $E_{GS} = 0$.

the p-shell, it follows that I should place 4 electrons on two p-shells; the symmetric and antisymmetric p-levels of the two-dot system. A sample configuration is shown in Figure 3.3. In total there are 70 configurations.

The results of diagonalization for a particular system with dots that are well-separated ($D = 3h$) are shown in Figure 3.4. The difference between the 9 lowest states and the Heisenberg spectrum is almost indistinguishable at this scale.

It would also be helpful to know the range of dot separations at which the Heisenberg spectrum is well-approximated. Ultimately the size of the Haldane gap depends on the strength of the Heisenberg interaction J, which I will later show to depend—for sufficiently well-separated dots that a Hubbard model is appropriate—predominantly on the symmetric-antisymmetric splitting (or tunneling coefficient). A study of this over a few distances is shown in Figure 3.5. I find that the approximation breaks down as I bring the dots closer together, but the spin-0 state remains the ground

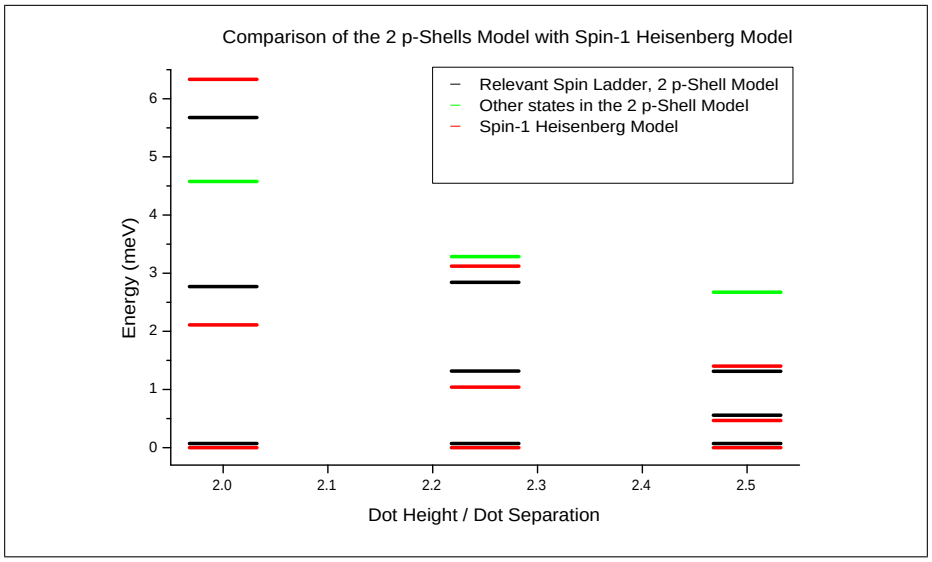

Figure 3.5: Comparison between the CI treatment of 4 electrons on 2 p-shells and the Heisenberg spin model for different dot separations. Degeneracy is not resolved. The black levels are $L = 0$ levels from CI; they are from lowest in energy to highest: the spin singlet, triplet, and quintuplet. The green levels are other levels from the CI spectrum. The Heisenberg J was fitted in the same manner as in Figure 3.4b.

state at any separation, and closer dots have a larger splitting from the spin-1 state and hence a larger effective J.

3.2.5 Double Quantum Dot with 8 Electrons

I am now ready to present a full CI treatment of 8 electrons distributed on the 12 single-particle levels of two quantum dots. As I have mentioned previously, such a system has a total of 735,471 configurations; the largest spin sub-basis (if I do not partition by L as well) has $245,025$. Fortunately the matrix is sparse (recall that configurations are only coupled if they contain at least 6 of the same electrons), and so the problem must be solved using iterative methods rather than direct diagonalization. Any large, sparse problem presented in this paper was solved using the Lanczos algorithm as implemented in ARPACK.

Based on results from the previous section—Figure 3.5 particularly—I decided to test two regimes; one where the Heisenberg Hamiltonian was very well approximated

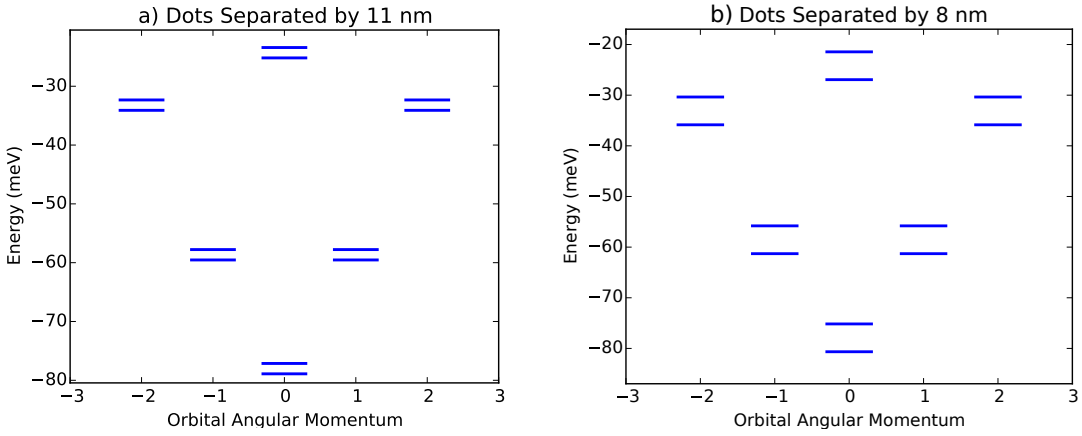

Figure 3.6: Single particle levels for the two systems with $R = a = 18$ nm and $h = 4$ nm. a) Dots separated by a 11 nm. b) dots separated by a 8 nm. The separation serves to increase the splitting between $|n, m, S\rangle$ and $|n, m, AS\rangle$ for each n, m.

(an 11 nm, or $2.75h$, dot separation), and one where the approximation broke down (an 8 nm, or $2h$, dot separation). The single-particle levels for both systems are shown in Figure 3.6.

The construction of the Hamiltonian takes a prohibitively long time without some optimization. In using the Lanczos algorithm I do not need to store nonzero matrix elements, but even explicitly calculating elements that are zero is not feasible when there are some 30 billion elements on the largest upper triangular. The bulk of the computation lies in determining the Coulomb term between two states, so minimizing calls to this routine is essential. Conservation of L can be enforced prior to making this computation, but the main speedup comes from enforcing the two configurations to differ by only two electrons.

While an algorithm which visits each site of the Hamiltonian at all—even if only to skip the site via the checks I have mentioned—is far from optimal, it suffices for my purposes in this section with the above optimizations.

The Lanczos method computes only a few of the lowest eigenvalues for each spin (say, 100). It will so happen that, *e.g.*, the $S_z = 0$ subspace will run through these levels before reaching any levels present in $S_z = 4$. I account for this by checking

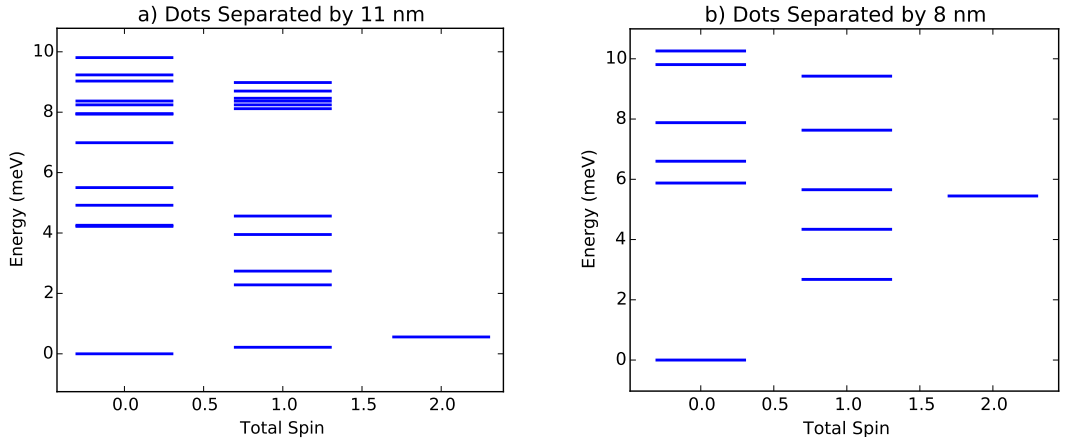

Figure 3.7: Lowest several energy levels for the full 8-electron CI treatment of the two-dot system. a) 11 nm dot separation. Note that there is a relatively well-isolated spin ladder as was the case when only considering p-shell electrons. b) 8 nm dot separation. Note that as in the treatment restricted to the p-shell, at this separation there are other states at lower energies than some of those in the spin ladder, but the ground state is spin-0 nonetheless.

in reverse order (starting at $S_z = 4$) for degeneracies; if the lower subspaces go far enough to contain degeneracies they can be accounted for in this manner.

Further, I do not show levels for $S = 3$ or 4. They occur $\sim$30 meV or so above the ground state of each system due to the fact that it is impossible to arrange 8 electrons on the 12 states with 6 or more in the same polarization without occupying the d-shell, which is comparatively very high in energy.

The few lowest levels (out to $\sim$10 meV) are shown in Figures 3.7. At least as far as the spin ladder is concerned, one sees the same general features as in the limited basis only accounting for the p-shell; for the well-separated dots, the spin-ladder is well-separated, but the magnitude of the effective Heisenberg J is quite low. For closer dots, we get better isolation of the spin-0 ground state, but the effective Heisenberg model is not a particularly good approximation.

A closer view of the spin ladder for the 11 nm case is shown in Figure 3.8, with some discussion as to the degree at which the system approximates the Heisenberg ladder. All things considered, the Heisenberg model is certainly very well approximated in

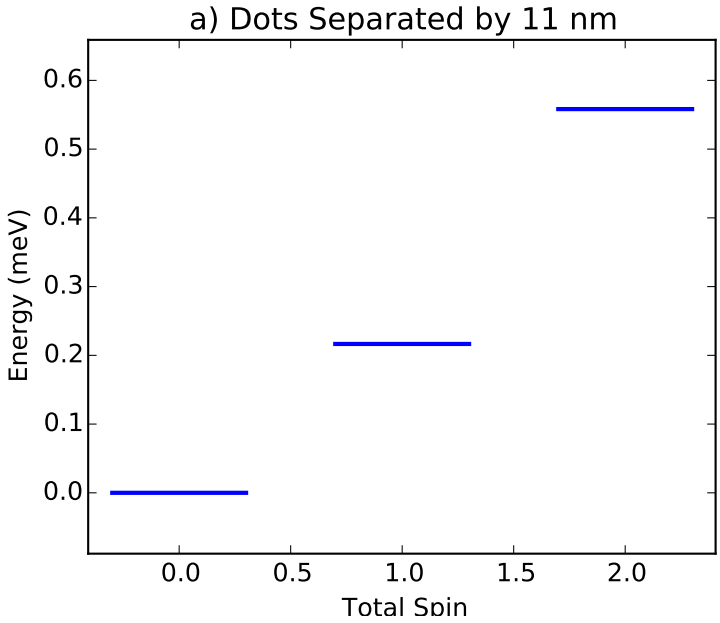

Figure 3.8: Closer view of the 11 nm lowest three levels. A Heisenberg model is approximately correct, but there is clear deviance from a step of J followed by another of $2J$).

the case of well-separated dots. That is to say, dot separation has some impact on the validity of the approximation, all else being equal. There is some indication that the strength of the effective J (which in turn determines the size of the Haldane gap) is also dependent on dot separation, all else being equal. To study this in better detail I turn to a simpler model that I can solve analytically.

3.3 Interacting Spin Model

To determine to first approximation what parameters control the validity and strength of the Heisenberg model as it pertains to my system, I will turn to a model of interacting spin-1/2 objects. The idea is that there are essentially two spins on each dot interacting with each other ferromagnetically via an effective J_1 (determined by the singlet-triplet splitting in the dot), and these electrons in turn interact across dots via an antiferromagnetic $J_2 << J_1$. Further, the electrons are occupying p-shells (from

whence the spin-interaction originates, as I have shown earlier). I will assume the intradot interaction only occurs between spins on the same m. I will label the sites as L or R for if they are on the left or right dot respectively, and $\pm$ for $m = \pm 1$. Then, for example, the spin on the left dot with $m = 1$ is $\boldsymbol{\sigma}_{L+}$. I will want a well-ordered set for my basis vectors so I will set

$$\{L+, L-, R+, R-\} \equiv \{1, 2, 3, 4\}. \tag{3.47}$$

Putting it all together, the Hamiltonian is

$$H_{sp} = -J_1 \left(\boldsymbol{\sigma}_1 \cdot \boldsymbol{\sigma}_2 + \boldsymbol{\sigma}_3 \cdot \boldsymbol{\sigma}_4\right) + J_2 \left(\boldsymbol{\sigma}_1 \cdot \boldsymbol{\sigma}_3 + \boldsymbol{\sigma}_2 \cdot \boldsymbol{\sigma}_4\right) \tag{3.48}$$

where I have chosen to parameterize J_1 and J_2 so as to use Pauli matrices

$$[\sigma^x, \sigma^y, \sigma^z] = \left[\begin{pmatrix} 0 & 1 \\ 1 & 0 \end{pmatrix}, \begin{pmatrix} 0 & -i \\ i & 0 \end{pmatrix}, \begin{pmatrix} 1 & 0 \\ 0 & -1 \end{pmatrix}\right] \tag{3.49}$$

instead of carrying the factors of $1/2$ throughout.

I will also choose to work in the computational basis

$$\{|0\rangle, |1\rangle\} \equiv \{|\uparrow\rangle, |\downarrow\rangle\} \tag{3.50}$$

for notational simplicity.

I can work in first quantization since the spins are distinguishable by virtue of their other quantum numbers; I need not worry about exchange symmetry. That is to say, states will be of the form *e.g.* $|0100\rangle$, where the first number is the spin on state 1, etc.

The operator

$$\boldsymbol{\sigma}_j \cdot \boldsymbol{\sigma}_k = \sigma_j^x \sigma_k^x + \sigma_j^y \sigma_k^y + \sigma_j^z \sigma_k^z \tag{3.51}$$

is an easy one to work out (indeed, it is a textbook problem). It may be helpful to explicitly enumerate the two-spin basis;

$$\{|0,0\rangle, |0,1\rangle, |1,0\rangle, |1,1\rangle\}. \tag{3.52}$$

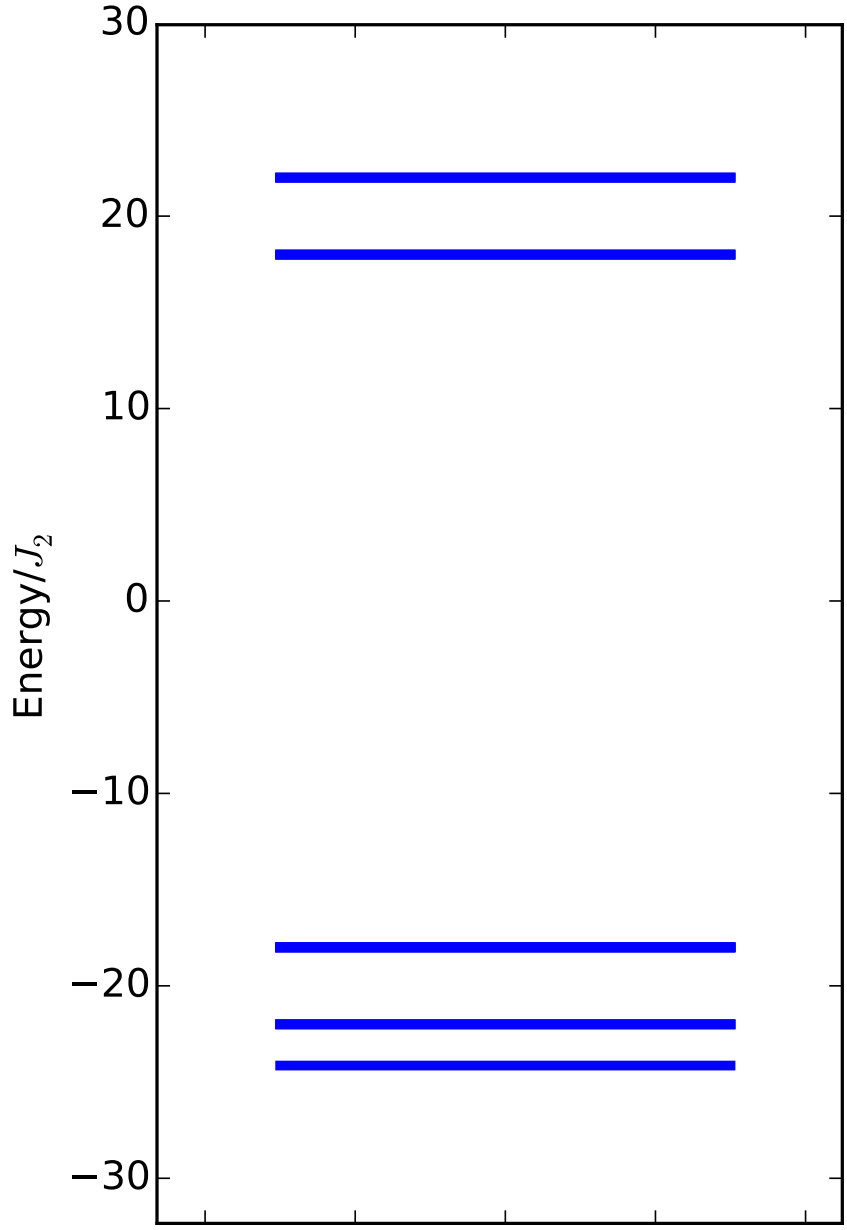

Figure 3.9: Spectrum of the 4-spin model (excluding an $S = 0$ state above $60J_2$) with $J_1/J_2 = 10$. The bottom three lines are almost identically the Heisenberg spectrum save for a discrepancy Δ, they are with a singlet at $-2(J_1 + 2J_2) - \Delta$, a triplet at $-2(J_1 + J_2)$, and a quintuplet at $-2(J_1 - J_2)$. The excitations are $4(J_1 - J_2)$ higher in energy. Δ is larger for systems with smaller J_1/J_2. Here $\Delta = 0.14$.

The diagonal is of course just the product of projections for spins j and k. It will be positive if they are aligned and negative if they are not. Explicitly,

$$\sigma_j^z \sigma_k^z \left|j,k\right\rangle = \begin{cases} \left|j,k\right\rangle, & j = k; \\ -\left|j,k\right\rangle, & j \neq k. \end{cases} \tag{3.53}$$

For example, $\sigma_j^z \sigma_k^z \left|0,0\right\rangle = (1)(1)\left|0,0\right\rangle = \left|0,0\right\rangle$.

For the off-diagonal I will make use of addition modulo 2, denoted $\oplus$, in order to work on a general state; $\left|0 \oplus 1\right\rangle = \left|1\right\rangle$ and $\left|1 \oplus 1\right\rangle = \left|0\right\rangle$. The important aspect of this is that the action of σ_i^x and σ_i^y is to flip the i^{th} spin *regardless of its initial orientation*. Using this notation I can derive the off-diagonal component of any two-spin polarization;

$$\begin{aligned} \left(\sigma_j^x \sigma_k^x + \sigma_j^y \sigma_k^y\right)\left|j,k\right\rangle &= \left|j \oplus 1, k \oplus 1\right\rangle + (-1)^j (-1)^k \cdot i^2 \left|j \oplus 1, k \oplus 1\right\rangle \\ &= \left|j \oplus 1, k \oplus 1\right\rangle + (-1)^{j+k+1}\left|j \oplus 1, k \oplus 1\right\rangle, \end{aligned} \tag{3.54}$$

Which very nicely reduces to

$$\left(\sigma_j^x \sigma_k^x + \sigma_j^y \sigma_k^y\right)\left|j,k\right\rangle = \begin{cases} 2\left|k,j\right\rangle, & j \neq k; \\ 0, & j = k. \end{cases} \tag{3.55}$$

That is, the σ^x and σ^y only connect $\left|01\right\rangle$ to $\left|10\right\rangle$, preserving total S_z as they should.

In full, the two-spin Hamiltonian in basis (3.52) is

$$\boldsymbol{\sigma}_j \cdot \boldsymbol{\sigma}_k = \begin{pmatrix} 1 & 0 & 0 & 0 \\ 0 & -1 & 2 & 0 \\ 0 & 2 & -1 & 0 \\ 0 & 0 & 0 & 1 \end{pmatrix}. \tag{3.56}$$

I can now one by one apply the two-spin operators present in the full Hamiltonian, acting on the appropriate two spins, to generate its matrix representation.

Figure 3.9 shows the spectrum for $J_1/J_2 = 10$. J_2 uniquely determines the effective Heisenberg J of a spin-1 model (it is $2J_2$), while J_1/J_2 determines the validity of that model. A larger ratio J_1/J_2 pushes the singlet state E_S further from its expected value of $E_T - 2J$ (where E_T is the triplet energy); shown in Figure 3.10.

In short, this model accurately reproduces the Heisenberg spin-1 ladder when $J_1 >> J_2$.

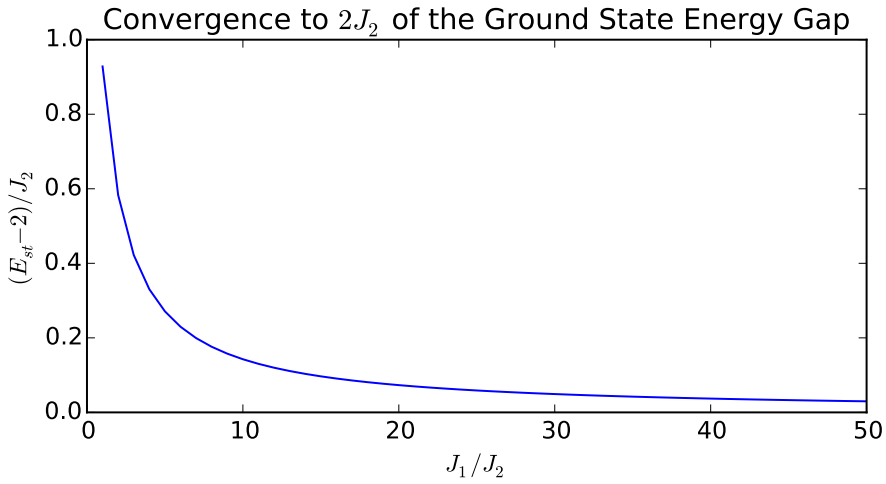

Figure 3.10: The difference between the singlet-triplet splitting in this model and the one expected in a Heisenberg model (the quantity Δ in the description of Figure 3.9) as a function of J_1/J_2. When the ratio becomes arbitrarily large, the Heisenberg spectrum is recovered exactly.

3.3.1 Origin of Heisenberg J

I will now determine the origin of J_2 and hence the spin-1 J in this simple model (we already understand the origin of J_1 as being the singlet-triplet splitting on a single dot, which is determined by the strength of the Coulomb matrix elements—and especially the exchange in the p-shell—on the dot) so that ultimately a system can be designed so as to maximize it and by consequence the Haldane gap.

A deeper model is needed to understand this. I will look at the interaction between quantum dots that each contain a single state, namely the $p+$ or $p-$ levels individually, which give rise to the J_2 interaction in my simplified spin model. I will assume that there are two electrons ditributed on the $p+$ (or $p-$) level of each dot, free to occupy either state obeying Pauli exclusion.

I will use the Hubbard Hamiltonian[19][21] to describe the interaction;

$$H = -t \sum_{i \neq j} c^{+}_{i\sigma} c_{j\sigma} + U \sum_{i} n_{i\uparrow} n_{i\downarrow}, \tag{3.57}$$

where $i, j \in \{L, R\}$ indicates on which dot the electron resides, t is the hopping matrix

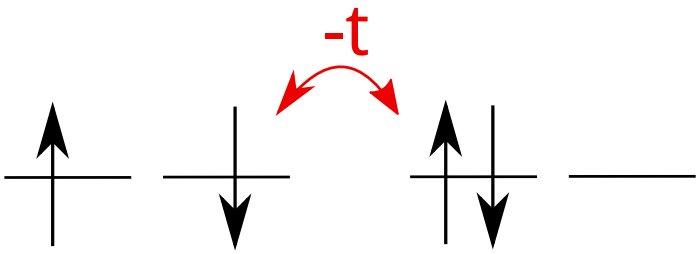

Figure 3.11: Two configurations connected via the hopping matrix element. An electron may move from the left dot to the right dot if it is not excluded by a like spin. The right configuration has a nonzero onsite term contributing $+U$ to the energy of the configuration.

element derived in Section 2.5, U is the onsite direct Coulomb element for the state, and

$$n_{i\sigma} = c^+_{i\sigma} c_{i\sigma} \tag{3.58}$$

is the number operator for a given state; the term is nonzero only if the state is occupied in a given configuration, where its eigenvalue is 1. In this way the second term makes it energetically unfavorable for a dot to be doubly-occupied (typically $U >> t$; indeed, all of the systems I have looked at thus far have exhibited this property). The hopping mechanism is illustrated in Figure 3.11.

The spin-polarized ($S_z = 1$) basis has only one configuration, $c^+_{L\uparrow} c^+_{R\uparrow} |0\rangle$. Its energy is given by

$$-t \sum_{i \neq j} c^+_{i\sigma} c_{j\sigma} c^+_{L\uparrow} c^+_{R\uparrow} |0\rangle + U \sum_i n_{i\uparrow} n_{i\downarrow} c^+_{L\uparrow} c^+_{R\uparrow} |0\rangle \tag{3.59}$$

which is easily seen to be zero; the first term is strictly off-diagonal and there is no double occupation for the second term to count.

The Hubbard Hamiltonian, much like the full interacting Hamiltonian it approximates, preserves S_z and S^2. It will be helpful to work in the basis of their eigenvalues collectively, so as to eliminate the $S_z = 0$ triplet state right away. The basis of

$|S=0, S_z=0\rangle$ levels consists of the spin singlet and the two doubly-occupied configurations;

$$|1\rangle \equiv \frac{1}{\sqrt{2}}\left(c^+_{L\uparrow}c^+_{R\downarrow} - c^+_{L\downarrow}c^+_{R\uparrow}\right)|0\rangle \tag{3.60a}$$

$$|2\rangle \equiv c^+_{L\uparrow}c^+_{L\downarrow}|0\rangle \tag{3.60b}$$

$$|3\rangle \equiv c^+_{R\uparrow}c^+_{R\downarrow}|0\rangle \tag{3.60c}$$

It should be noted that this is not an eigenbasis of the Hamiltonian as hopping connects the singlet to the two doubly-occupied states. The doubly-occupied configurations have energy $+U$, while the singlet has $E_S = 0$. I will now expand the ground state of the diagonal onsite term (the singlet) in t as a perturbation; to second order:

$$\begin{aligned} E_{GS} &= E_1^{(0)} - t\langle 1|V|1\rangle + t^2 \sum_{n\neq 1} \frac{|\langle n|V|1\rangle|^2}{E_0 - E_n} + O(t^3) \\ &= t^2 \sum_{n\neq 1} \frac{|\langle n|V|1\rangle|^2}{(-U)} + O(t^3) \end{aligned} \tag{3.61}$$

where

$$V = \sum_{i\neq j} c^+_{i\sigma}c_{j\sigma}. \tag{3.62}$$

Due to the symmetry of the problem the matrix element will be the same for state $|2\rangle$ as it is for state $|3\rangle$;

$$\langle 2|V|1\rangle = \frac{1}{\sqrt{2}}\left\langle 0\middle| c_{L\downarrow}c_{L\uparrow}\sum_{i\neq j} c^+_{i\sigma}c_{j\sigma}\left(c^+_{L\uparrow}c^+_{R\downarrow} - c^+_{L\downarrow}c^+_{R\uparrow}\right)\middle|0\right\rangle$$

where in both terms I must have $i = L, j = R$ with like spins left over for a nonzero outcome; the first term requiring two permutations and the second requiring one, leaving

$$\begin{aligned} \langle 2|V|1\rangle &= \frac{1}{\sqrt{2}}\left\langle 0\middle| c_{L\uparrow}c^+_{L\uparrow} + c_{L\downarrow}c^+_{L\downarrow}\middle|0\right\rangle \\ \langle 2|V|1\rangle &= \frac{1}{\sqrt{2}}\left(\langle 0|0\rangle + \langle 0|0\rangle\right) \\ \langle 2|V|1\rangle &= \sqrt{2}. \end{aligned} \tag{3.63}$$

The term comes up twice in the sum of the perturbation expansion (3.61) (for $n = 2$ and 3), leaving me with

$$\begin{aligned} E_{GS} &= -t^2 \cdot 2\frac{\left|\sqrt{2}\right|^2}{U} + O(t^3) \\ &\approx -\frac{4t^2}{U}. \end{aligned} \tag{3.64}$$

Recalling that the triplet energy was 0; the singlet energy is lower. J_2 is defined by this singlet-triplet splitting, and so

$$J_2 \propto \frac{t^2}{U}. \tag{3.65}$$

The singlet is the ground state so the interaction is antiferromagnetic as expected. In this simple model, the antiferromagnetic J_2, and thus the effective spin-1 Heisenberg J and the Haldane gap, depend solely on the tight-binding tunneling parameter between p-shells of the two dots (approximately the symmetric-antisymmetric splitting) and its strength compared to the onsite Coulomb direct term U, which is greater than but on the order of J_1 (recall that we required $J_2 << J_1$ for the spin-1/2 system to approximate the Heisenberg Hamiltonian; here we require exactly the same circumstance via $t << U$).

Now, I showed back in Section 2.4 that t is completely determined by dot separation. Thus, for a given system, dot separation controls the size of the Haldane gap insofar as $t << U$. It is well-understood how to tune the parameters of a single dot in order to, *e.g.*, control the scale of Coulomb interactions as compared to level spacing[20][30]. One can maximize the on-site exchange term in this way, allowing for a larger tunneling coefficient without breaking the approximation.

Chapter 4

Spin Chains and the Singlet-Triplet Qubit

I have now fully characterized the single and double quantum dots embedded in a nanowire in particular showing that the two-dot system can be well-approximated by the Heisenberg Hamiltonian under certain conditions. I have further broken the Heisenberg model into the interaction of spin-1/2 quasiparticles, two on each dot, forming triplets within a dot and singlets between dots. From this model, and an analysis of its origin, I was able to determine the parameters controlling the strength and validity of the Heisenberg Hamiltonian.

Now, for N-site chains with $N > 2$, a full electron interaction treatment becomes unfeasible. A 3-dot, 12-electron treatment like I have done in Section 3.2.5 has over a billion possible configurations. Even if that were tractable, going above 3 dots would certainly not be.

For this reason I will now work exclusively with the Heisenberg Hamiltonian for N-site spin-chains

$$H_1 = J \sum_{i=1}^{N-1} \boldsymbol{S}_i \cdot \boldsymbol{S}_{i+1} \tag{4.1}$$

and a model involving two spins-1/2 on each dot as in (3.48);

$$H_{1/2} = -J_1 \sum_{i=1}^{N} (\boldsymbol{\sigma}_{i,1} \cdot \boldsymbol{\sigma}_{i,2}) + J_2 \sum_{i=1}^{N-1} (\boldsymbol{\sigma}_{i,1} \cdot \boldsymbol{\sigma}_{i+1,1} + \boldsymbol{\sigma}_{i,2} \cdot \boldsymbol{\sigma}_{i+1,2}), \tag{4.2}$$

to perform finite-chain calculations in order to

1. Verify the 4-fold degenerate ground state and the size of the Haldane gap;
2. Show convergence of (4.2) to (4.1) in the limit $J1 >> J2$;
3. Determine how to manipulate the 4-fold degenerate ground-state as a singlet-triplet qubit.

4.1 Finite Chain Calculations of the Heisenberg Hamiltonian

Many finite-chain calculations of the spin-1 chain have been done already[3][5][7]. I will verify the low-energy spectrum as a function of N lattice sites as well as the behaviour of the spin-polarized low-energy levels with my own finite-chain calculations, and then extend the Hamiltonian to include localized magnetic fields in order to realize a singlet-triplet qubit.

For a chain of any length I can just go through each configuration and apply the pairwise Hamiltonians from Section 3.2.3 to each configuration, in this way generating the full Hamiltonian.

Working with chains $N > 2$ causes the basis to grow exponentially. Each site can have three polarizations; there are 3^N total configurations. The Hamiltonian must be diagonalized as a sparse Hamiltonian after about $N = 8$, and must be constructed very efficiently after $N = 12$ or so.

To this end I am actually able to construct the Hamiltonian in $O(n_{nz})$ operations (for n_{nz} matrix elements). The naive algorithm visiting every matrix element is $O(n^2)$ (for n configurations), and even when automatically skipping known zero elements is not practical for very long chains. What I do is construct the basis from the fully negatively polarized configuration through the fully positively polarized configuration ordered so as to increment the rightmost spin first. I then apply the Hamiltonian to each state in the basis, generating one or several new configurations. I can do this one $\boldsymbol{S}_i \cdot \boldsymbol{S}_j$ at a time because these pairwise Hamiltonians necessarily generate

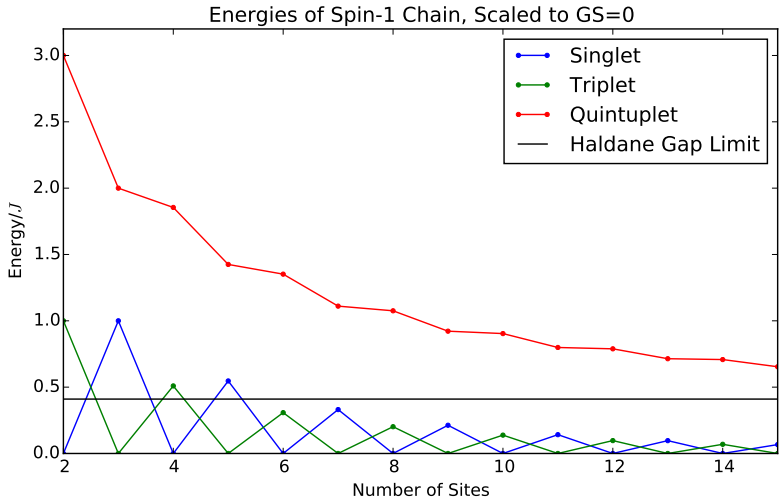

Figure 4.1: Singlet, triplet and quintuplet states in finite chains of N sites. In the $N \to \infty$ limit, the singlet and triplet are degenerate, and the quintuplet exists at $\sim +41J$, predicted based on Monte-Carlo and DMRG calculations for chains much longer than this[31][6].

unique states from one another ($\boldsymbol{S}_1 \cdot \boldsymbol{S}_2$ does not touch the spin on site 3, and so on). I do not need to look up these configurations, which is computationally costly, because they are uniquely identified by base-3 arithmetic (with the polarizations $\{-1, 0, 1\}$ mapped onto base-3 $\{0, 1, 2\}$). For example when $N = 3$, $|-1, 1, 0\rangle$ is the $0(3^2) + 2(3^1) + 1(3^0) = 8^{\text{th}}$ configuration (counting from 0).

The result of finite chain calculations for $N \in \{2, 3, \ldots, 15\}$ is shown in Figure 4.1. The calculation agrees nicely with previous results[5][31]; namely, the singlet and triplet become closer in energy, their ordering oscillating with N, while the quintuplet appears to approach a finite energy. It is also interesting to look at $\langle S_i^z \rangle$, that is, the polarization of a given site (for $S_{tot}^z = 1$ states that is; if $S_{tot}^z = 0$ this is identically 0 at every site due to every imaginable configuration having an equivalent configration with all of the spins in the opposite polarization). $\langle S_i^z \rangle$ is shown in Figure 4.2. The edge-states in the $S_{tot}^z = \pm 1$ state tend to $\langle S_1^z \rangle = \langle S_N^z \rangle \approx \pm 1/2$, indicating a spin-1/2 character on the ends of the chain[7]. This will be the basis for manipulation of the qubit states in analogy with a singlet-triplet qubit as for example in ref. [9].

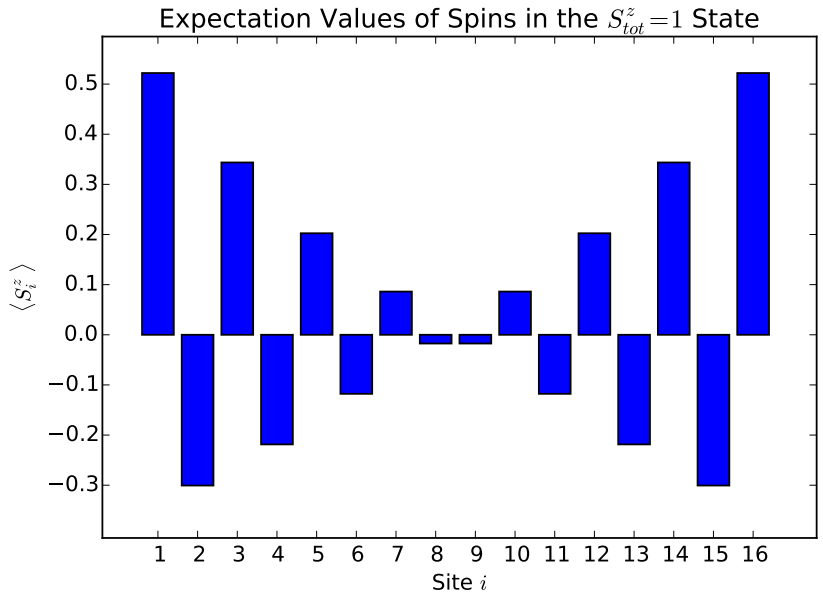

Figure 4.2: Expectation value of S_i^z for the $S = S_z = 1$ state at each site i for a 16-site chain. The edge states tend to $\langle S^z \rangle = 0.5$, and decay to 0 away from this. For $S_z = -1$, all bars in this graph are multiplied by -1.

4.1.1 Manipulation of Singlet-Triplet Qubit by B-Field

The singlet-triplet qubit is a subspace of the total $|S^2, S^z\rangle$ eigenbasis of two spins, the states of which are

$$|S_0\rangle = \frac{1}{\sqrt{2}} \left(|01\rangle - |10\rangle\right); \tag{4.3a}$$

$$|T_-\rangle = |00\rangle; \tag{4.3b}$$

$$|T_0\rangle = \frac{1}{\sqrt{2}} \left(|01\rangle + |10\rangle\right); \tag{4.3c}$$

$$|T_+\rangle = |11\rangle, \tag{4.3d}$$

where S_0 is spin-0 and the T are spin-1. These levels also diagonalize the 2-spin Heisenberg Hamiltonian for spins-1/2; shifted to make the ground state have zero energy, the eigenvalues are

$$J\boldsymbol{\sigma}_1 \cdot \boldsymbol{\sigma}_2 \, |S, S_z\rangle = \begin{cases} 0, & S = 0; \\ 4J, & S = 1, \end{cases} \tag{4.4}$$

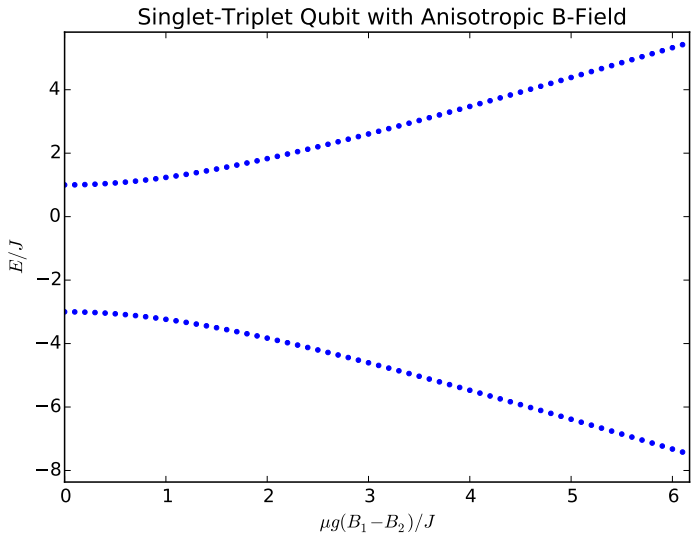

Figure 4.3: The S_0 and T_0 levels interact when an anisotropic magnetic field is applied to a two-spin system. The levels repel one another with increasing anisotopy. B_i is the magnetic field on the i^{th} particle.

where $\boldsymbol{\sigma}_i$ are Pauli matrices.

The sub-basis

$$\{|S_0\rangle, |T_0\rangle\} \tag{4.5}$$

is the singlet-triplet qubit. It will need to be isolated from the remainder of the basis; to this end one introduces a uniform magnetic field

$$H = J\boldsymbol{\sigma}_1 \cdot \boldsymbol{\sigma}_2 + \mu g B_{bg} S^z, \tag{4.6}$$

where g is the Landé g-factor and μ is the effective Bohr magneton. Since S^z is a good quantum number this serves only to split the levels by the Zeeman energy $\mu g B_{bg}$. $|T_\pm\rangle$ have finite S^z so are split off from the qubit states which are unaffected;

$$E_{S,S^z} = \mu g B_{bg} S^z + 4J\delta_{S,1}. \tag{4.7}$$

if the Zeeman term $\mu g B_{bg}$ is sufficiently stronger than J one can in this way effectively isolate the qubit states $|S_0\rangle$ and $|T_0\rangle$. The Hamiltonian (4.7) in the qubit sub-basis (4.5) is

$$H = \begin{pmatrix} 0 & 0 \\ 0 & 4J \end{pmatrix}. \tag{4.8}$$

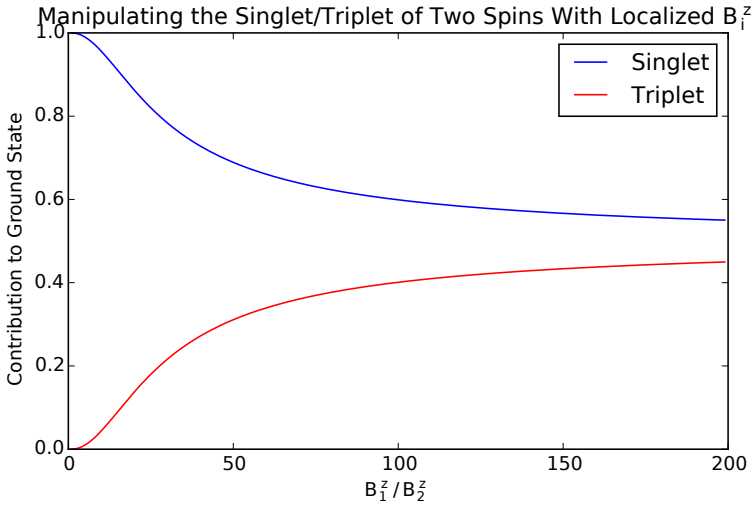

Figure 4.4: Projection (squared) of the ground state onto the singlet and triplet configurations S_0 and T_0. In the limit $B_1^z \to \infty$, they each attain a value of 0.5, which is to say S_i^z become good quantum numbers. The quantity B_1^z/B_2^z on the x-axis takes into account B_{bg} and so $B_1^z/B_2^z = 1$ is the no anisotropy case.

Now, if I introduce anisotropy in the magnetic field such that

$$H_{st} = J\boldsymbol{\sigma}_1 \cdot \boldsymbol{\sigma}_2 + \mu g(B_{bg}S^z + B_1 S_1^z), \tag{4.9}$$

the qubit states will be mixed;

$$\frac{1}{\sqrt{2}}\hat{S}_1^z\left(|01\rangle \pm |10\rangle\right) = \frac{1}{\sqrt{2}}\left(\frac{1}{2}|01\rangle \mp \frac{1}{2}|10\rangle\right). \tag{4.10}$$

The Hamiltonian is now

$$H_{st} = \begin{pmatrix} 0 & \frac{1}{2}\mu g B_1 \\ \frac{1}{2}\mu g B_1 & 4J \end{pmatrix}. \tag{4.11}$$

The eigenvalues of this Hamiltonian repel with increasing B_1 (Figure 4.3). They are admixtures of the singlet and triplet, and in the limit $B_1 \to \infty$ they become the $|S_1^z, S_2^z\rangle$ eigenstates $|01\rangle$ and $|10\rangle$. Projections onto the singlet and triplet are shown in Figure 4.4.

This simple analysis is straightforwardly generalized to a chain of N spins-1. Recall that the spin-1 chain formed $S^z = 0.5$ edge states at low energy, hence one can think

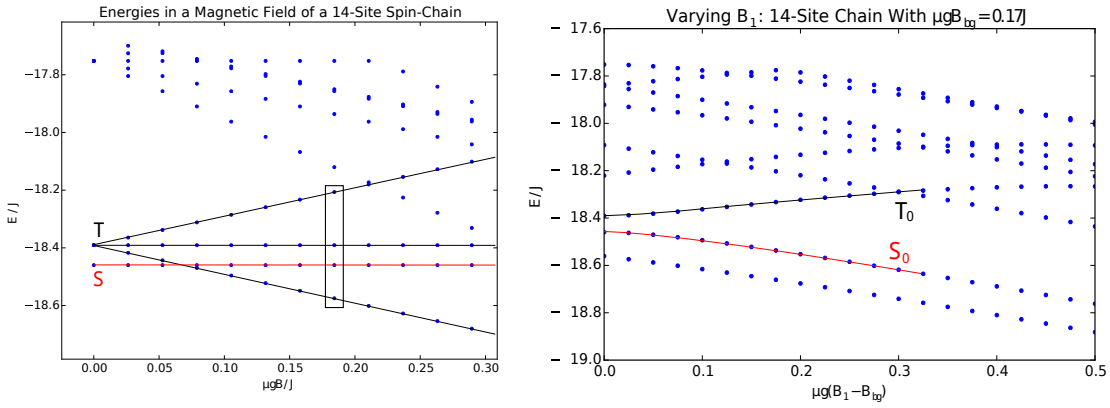

Figure 4.5: Varying B-fields on a 14-site spin-1 chain. Left: varying the background field to split off $T_\pm$ from the singlet-triplet qubit. Right: Varying B_1 to break the S^2 symmetry and cause $|S_0\rangle$ and $|T_0\rangle$ to interact. At sufficiently low energies, these levels appear to repel one-another; at higher energies the interaction with the $|Q_0\rangle$ quintuplet state and other outlying states appears to become important.

of the chain as two spins-1/2 in this regime. The goal now is to make the $|S_0\rangle$ and $|T_0\rangle$ states below the Haldane gap interact.

One might first think of following the exact same procedure, namely applying a uniform magnetic field to each spin and an anisotropy affecting only the first dot, such that

$$H = J\sum_{i=1}^{N-1} \boldsymbol{S}_i \cdot \boldsymbol{S}_{i+1} + \sum_{i=1}^{N} \mu g B_{bg} S_i^z + \mu g B_1 S_1^z. \tag{4.12}$$

Some key points should be made about the similarity, particularly in regard to the quantum numbers of the system: as in the two-spin case, S^2 is no longer a good quantum number because it does not commute with S_1^z, however $S^z = \sum_i S_i^z$ is still a good quantum number.

It follows that $|S_0\rangle$ and $|T_0\rangle$ in the spin chain (in this case, the $S_z = 0$ projection of the lowest-energy singlet and triplet of the spin chain) will interact, and independently of $|T_\pm\rangle$. There will be some small admixture of other states with $S_z = 0$; however, due to the Haldane gap these are relatively quite far in energy from the singlet and triplet state. Based on this relatively short, heuristic analysis I should expect that I can manipulate the qubit in such a way, and indeed this turns out to work very well.

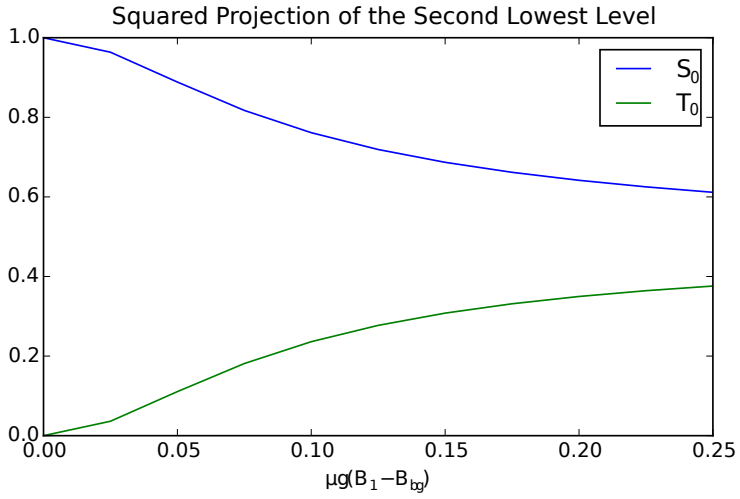

Figure 4.6: Projection (squared) of the second lowest level shown in Figure 4.5 ($|S_0\rangle$ at $B_1 = 0$) onto $|S_0\rangle$ and $|T_0\rangle$ of the chain, showing excellent agreement with the two-spin case. This is the analogy in this system of Figure 4.4. Admixture of higher levels is less than 1.3% at the far right of this figure.

I proceed on a spin-chain with $N = 14$ sites. I first want to sufficiently isolate the $S_z = 0$ states; this is done with the B_{bg} term in (4.12);

$$H = J\sum_{i=1}^{13} \boldsymbol{S}_i \cdot \boldsymbol{S}_{i+1} + \sum_{i=1}^{14} \mu g B_{bg} S_i^z \tag{4.13}$$

in a regime where the $|S_0\rangle$, $|T_0\rangle$ are appropriately isolated from $|T_\pm\rangle$. I then turn on the nonuniform field B_1 to mix them; the Hamiltonian is now the full (4.12). The evolution of both processes is shown in Figure 4.5, while the projections onto $|S_0\rangle$ and $|T_0\rangle$ in the nonuniform field are shown in Figure 4.6. The agreement with the two-spin case is very good, and it appears the singlet-triplet qubit is perfectly valid in this system.

4.2 Interaction of Spin-1/2's on a Lattice

It is a good idea to briefly compare with a model that more closely resembles an actual system. This model is the interacting spins-1/2 on a lattice of Section 3.3,

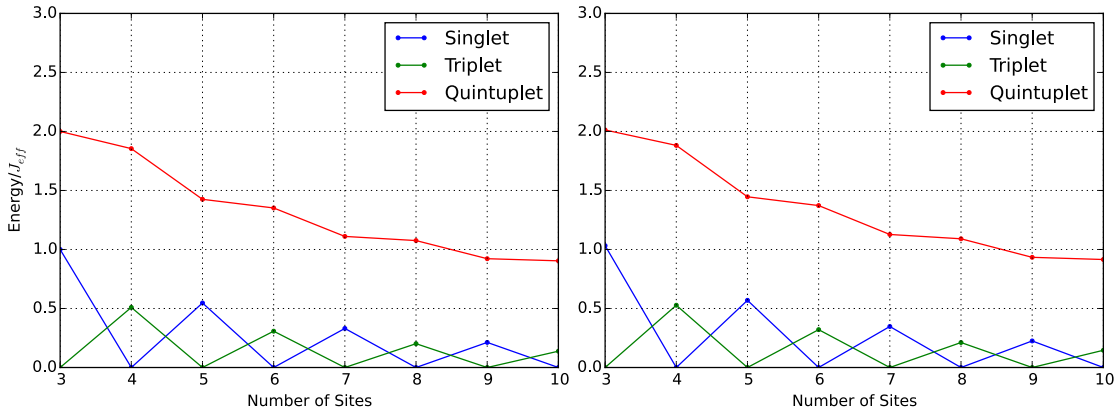

Figure 4.7: Comparing the $S = 1$ Heisenberg spin-chain (left) with the coupled spins-1/2 chain (right), where $J_1/J_2 = 25$. The states of interest are nearly indistinguishable. Here, J_{eff} is just J in the case of the spin-1 chain, and $J_2/2$ in the localized spin-1/2 case.

extended to multiple sites:

$$H_{1/2} = -J_1 \sum_{i=1}^{N} (\boldsymbol{\sigma}_{i,+} \cdot \boldsymbol{\sigma}_{i,-}) + J_2 \sum_{i=1}^{N-1} (\boldsymbol{\sigma}_{i,+} \cdot \boldsymbol{\sigma}_{i+1,+} + \boldsymbol{\sigma}_{i,-} \cdot \boldsymbol{\sigma}_{i+1,-}), \tag{4.14}$$

where $\boldsymbol{S}_{i,\pm}$ is a spin localized on the $p\pm$ orbital of the i^{th} dot. I solved the two-site Hamiltonian back in section 3.3, and I will now proceed in exactly the same way as I did with the spin-1 Heisenberg Hamiltonian, with some obvious differences. For one, the pairwise Hamiltonians are different. There are also 4^N configurations for N sites; this grows much more quickly than 3^N. Each configuration is still uniquely identified (though modulo 2 this time) eliminating once again the need for lookup of matrix elements.

First it is worth checking whether the model agrees when $J_1 >> J_2$, as I have shown that it should. Indeed, where this is the case, the relevant part of the spectrum is indistinguishable (Figure 4.7).

It is worth noting that the approximation remains quite good even when $J_1/J_2 \approx 3$ or so, as can be seen in Figure 4.8.

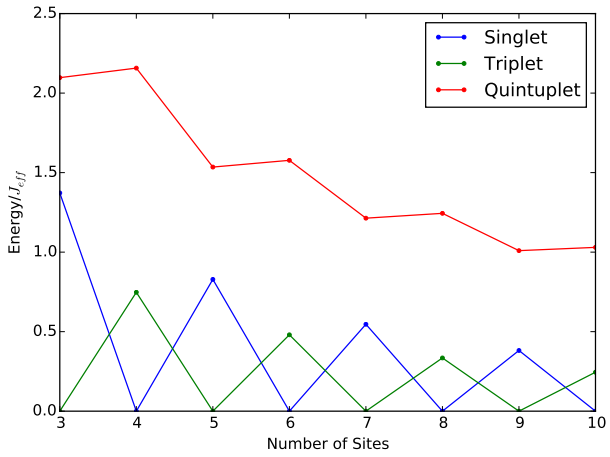

Figure 4.8: The localized spin-1/2 chain with $J_1/J_2 = 3$. We still see a gap, and the ground state appears to still converge to degeneracy, but the approximation to the spin-1 case is rougher; in particular, note that for an even chain N, the odd $N+1$ chain has higher energies all around, which we did not see before.

4.2.1 Tuning of the Ground State by Number of Sites

We had expected that since an even chain is $S = 0$ and an odd chain is $S = 1$, perhaps we could manipulate the singlet and triplet levels by changing J_2 between the first and second dot only, so that

$$H_{1/2} = -J_1 \sum_{i=1}^{N} (\boldsymbol{\sigma}_{i,+} \cdot \boldsymbol{\sigma}_{i,-}) + \Delta_i J_2 \sum_{i=1}^{N-1} (\boldsymbol{\sigma}_{i,+} \cdot \boldsymbol{\sigma}_{i+1,+} + \boldsymbol{\sigma}_{i,-} \cdot \boldsymbol{\sigma}_{i+1,-}), \tag{4.15}$$

where

$$\Delta_i = \begin{cases} \epsilon, & i = 1; \\ 1, & \text{otherwise}; \end{cases} \tag{4.16}$$

for $\epsilon \leq 1$. The endpoint behaviour is understood; for $\epsilon = 1$ we have identical results to the N-site chain, while for $\epsilon = 0$ we expect to see the same level ordering and spacing as for an $N-1$ chain, except with an extra 3-fold degeneracy factor from the isolated spin, which prefers to be a triplet. However, the behaviour between these values is not immediately obvious, and if the levels cross (or the S^2 degeneracy is broken) this is a potentially useful means of manipulating the qubits.

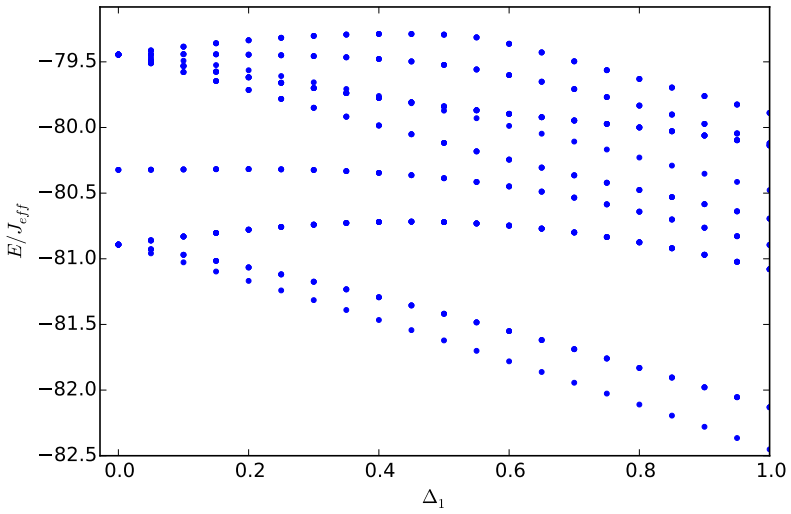

Figure 4.9: Varying ϵ in the system shown in Figure 4.7. There is no crossing of the singlet and triplet Haldane gap states. On the right, the levels are, in ascending energy, $S = (0, 1, 2, 1, 1, 0, 2, 1, 1)$; these coalesce on the left into the new $S = (1, 0, 2)$ states of the odd chain. Only the singlet and quintuplet near the top of this figure cross.

The evolution of this spectrum as a function of Δ_1 is shown in Figure 4.9. In short, the singlet and triplet do not cross; the ordering persists for any finite Δ_1. Further, S^2 remains a good quantum number, which can probably be rigourously proved. Of note is that the Haldane gap system (the lowest 9 levels) coalesce to become the 9 levels corresponding to the spin-triplet on the $(N-1)$-chain, made threefold degenerate by the end spin-1. However, it does not appear that we can manipulate the qubit states simply by lowering interaction with the last dot.

Chapter 5

Conclusions

In summary, I have presented a model system of semiconductor quantum dots in a nanowire with 4 electrons each, that is a good candidate for a Haldane gap material. Under suitable conditions, which appear to depend on dot separation, the antiferromagnetic Heisenberg Hamiltonian of two spins-1 can well-approximate two dots with 4 electrons each. I have shown that the strength of the Heisenberg exchange interaction J depends for a given dot size on the dot separation if a single-orbital tight-binding hybridization is appropriate.

Further, I have explored possibilities of manipulating the degenerate singlet-triplet ground state of the Haldane gap material; one can to some degree apply an anisotropic B-field to mix the two levels in much the same way one manipulates the singlet-triplet qubit of two spins. The singlet and triplet of a Haldane gap material are macroscopic quantum states; a point of particular interest. Ultimately, I have shown that quantum dots in nanowires may be a realizable macroscopic qubit.

5.1 Further Research

While I have used parameters somewhat typical of quantum dots grown at the National Research Council in Ottawa by Dalacu et al.[14], I have not attempted to optimize J in any way by tuning dot radius and height. Research into this could prove fruitful, as we speculate that room-temperature Haldane gaps might be achieved with

proper tuning of the dots, which is highly desirable.

Further work should first and foremost include atomistic calculations of the single-particle levels in the structures I have studied here. While the effective mass approximation can often elicit the salient features of a nanostructure, atomistic calculations will almost always introduce features that have not been accounted for; for example the breaking of the cylindrical symmetry (and hence splitting of the p-shell) due to the discreteness of the real system.

This work lacks any treatment of holes, which are an inescapable feature of any semiconducting system, and necessary if optical properties are desired.

Beyond refinement of these results, further effort could also be spent on better understanding how one might manipulate such a spin-chain. In particular, very large and localized magnetic fields are experimentally challenging to implement. Further, it is important to know how this qubit system could be probed. Optical properties of the system are important as well; how can the singlet-triplet qubit be converted into photons? These and many more questions are unresolved.

Bibliography

[1] F. D. M. Haldane. Nonlinear field theory of large-spin Heisenberg antiferromagnets: semiclassically quantized solitons of the one-dimensional easy-axis Néel state. *Physical Review Letters*, 50(15):1153–1156, 1983.

[2] Ian Affleck, Tom Kennedy, Elliott H. Lieb, and Hal Tasaki. Valence bond ground states in isotropic quantum antiferromagnets. *Communications in Mathematical Physics*, 115(3):477–528, 1988.

[3] R. Botet, R. Jullien, and M. Kolb. Finite-size-scaling study of the spin-1 Heisenberg-Ising chain with uniaxial anisotropy. *Physical Review B*, 28(7):3914–3921, 1983.

[4] W. J. L. Buyers, R. M. Morra, R. L. Armstrong, M. J. Hogan, P. Gerlach, and K. Hirakawa. Experimental evidence for the Haldane gap in a spin-1 nearly isotropic, antiferromagnetic chain. *Physical Review Letters*, 56(4):371–374, 1986.

[5] Yun-Pil Shim, Anand Sharma, Chang-Yu Hsieh, and Pawel Hawrylak. Artificial Haldane gap material on a semiconductor chip. *Solid State Communications*, 150(41-42):2065–2068, nov 2010.

[6] Steven R. White and David A. Huse. Numerical renormalization-group study of low-lying eigenstates of the antiferromagnetic S=1 Heisenberg chain. *Physical Review B*, 48(6):3844–3852, 1993.

[7] F. Delgado, C. D. Batista, and J. Fernández-Rossier. Local probe of fractional edge states of S=1 Heisenberg spin chains. *Physical Review Letters*, 111(16):1–5, 2013.

[8] Marek Korkusinski and Pawel Hawrylak. Chapter 1: Coded Qubit Based on Electron Spin. In *World Scientific Review*. 2008.

[9] J. R. Petta, A. C. Johnson, J. M. Taylor, E. A. Laird, A. Yacoby, M. D. Lukin, C. M. Marcus, M. P. Hanson, and A. C. Gossard. Coherent manipulation of coupled electron spins in semiconductor quantum dots. *Science*, 309(5744):2180–2184, 2005.

[10] Arkadiusz Wojs and Pawel Hawrylak. Charging and infrared spectroscopy of self-assembled quantum dots in a magnetic field. *Physical review. B, Condensed matter*, 53(16):10841–10845, 1996.

[11] S. Tarucha, D. G. Austing, T. Honda, R. J. van der Hage, and L. P. Kouwenhoven. Shell filling and spin effects in a few electron quantum dot. *Physical Review Letters*, 77:3613–3616, Oct 1996.

[12] Marek Korkusiski. *Correlations in Semiconductor Quantum Dots*. PhD thesis, University of Ottawa, June 2004.

[13] S. Raymond, S. Studenikin, A. Sachrajda, Z. Wasilewski, S. J. Cheng, W. Sheng, P. Hawrylak, A. Babinski, M. Potemski, G. Ortner, and M. Bayer. Excitonic energy shell structure of self-assembled InGaAs/GaAs quantum dots. *Physical Review Letters*, 92(18):187402, 2004.

[14] Dan Dalacu, Khaled Mnaymneh, Jean Lapointe, Xiaohua Wu, Philip J. Poole, Gabriele Bulgarini, Val Zwiller, and Michael E Reimer. Ultraclean emission from InAsP quantum dots in defect-free wurtzite InP nanowires. *Nano letters*, 12(11):5919–23, nov 2012.

[15] Andreas Wensauer, Marek Korkusinski, and Pawel Hawrylak. Theory of the spin-singlet filling factor ν=2 quantum Hall droplet. *Physical Review B*, 67(3):035325, jan 2003.

[16] Pawel Hawrylak. Excitonic artificial atoms: Engineering optical properties of quantum dots. *Physical Review B*, 60(8):5597–5608, 1999.

[17] Gustavo A. Narvaez and Pawel Hawrylak. Effects of electron-electron interactions on excitonic absorption in charged self-assembled quantum dots. *Physical Review B*, 61(20):13753–62, 2000.

[18] M. Bayer, P. Hawrylak, K. Hinzer, S. Fafard, M. Korkusinski, Z. R. Wasilewski, O. Stern, and A. Forchel. Coupling and entangling of quantum states in quantum dot molecules. *Science*, 291(5503):451–453, 2001.

[19] Irene Puerto Gimenez, Marek Korkusiski, and Pawel Hawrylak. Linear combination of harmonic orbitals and configuration interaction method for the voltage control of exchange interaction in gated lateral quantum dot networks. *Physical Review B*, 76(7):075336, aug 2007.

[20] Chang-Yu Hsieh, Yun-Pil Shim, Marek Korkusiski, and Pawel Hawrylak. Physics of lateral triple quantum-dot molecules with controlled electron numbers. *Reports on Progress in Physics*, 75(11):114501, nov 2012.

[21] J. P. Nikkarila, M. Koskinen, S. M. Reimann, and M. Manninen. Magnetic phases of one-dimensional lattices with 2-4 fermions per site. *New Journal of Physics*, 10(6):63013, 2008.

[22] Juan Jose Palacios and Pawel Hawrylak. Correleated few-electron states in vertical double-quantum-dot systems. *Physical Review B*, 51(3):1769–1777, 1995.

[23] Marek Korkusiski and Pawel Hawrylak. Electronic structure of vertically stacked self-assembled quantum disks. *Physical Review B*, 63(19):195311, apr 2001.

[24] Eugene S. Kadantsev, Micha Zieliski, and Pawel Hawrylak. Band engineering in nanowires: Ab initio model of band edges modified by (111) biaxial strain in group IIIA-VA semiconductors. *Physical Review B*, 86(8):085411, aug 2012.

[25] Y. M. Niquet, A. Lherbier, N. H. Quang, X. Blase, and C. Delerue. Electronic structure of semiconductor nanowires. *Physical Review B*, 73(165319):1–13, 2006.

[26] M. Heiss, Y. Fontana, A. Gustafsson, G. Wust, C. Magen, D. D. O'Regan, J. W. Luo, B. Ketterer, S. Conesa-Boj, A. V. Kuhlmann, J. Houel, E. Russo-Averchi,

J. R. Morante, M. Cantoni, N. Marzari, J. Arbiol, A. Zunger, R. J. Warburton, and A. Fontcuberta i Morral. Self-assembled quantum dots in a nanowire system for quantum photonics. *Nature Materials*, 12(5):439–444, 2013.

[27] Pawel Hawrylak. Far infrared absorption by screened d-states in quantum wells in a strong magnetic field. *Solid State Communications*, 88(6):475–479, 1993.

[28] Weidong Sheng, Shun-Jen Cheng, and Pawel Hawrylak. Multiband theory of multi-exciton complexes in self-assembled quantum dots. *Physical Review B*, 71(3):035316, jan 2005.

[29] J.J. Sakurai and Jim Napolitano. *Modern Quantum Mechanics*. Pearson, 2nd edition, 2011.

[30] Weidong Sheng and Pawel Hawrylak. Atomistic theory of electronic and optical properties of InAs/InP self-assembled quantum dots on patterned substrates. *Physical Review B*, 72(3):035326, jul 2005.

[31] Ian Affleck. Quantum spin chains and the Haldane gap. *Journal of Physics: Condensed Matter*, 1(19):3047, 1989.